CAPITAL UNIVERSITY OF SCIENCE AND TECHNOLOGY, ISLAMABAD

Study and Simulations of Klystron Modulator Pulse Transformer

by

Waqas Ahmed Toor

A thesis submitted in partial fulfillment for the degree of Master of Science

in the

Faculty of Engineering
Department of Electrical Engineering

2019

This Thesis is dedicated to my family.

CERTIFICATE OF APPROVAL

Study and Simulations of Klystron Modulator Pulse Transformer

by

Waqas Ahmed Toor

(MEE161019)

THESIS EXAMINING COMMITTEE

S. No.	Examiner	Name	Organization
(a)	External Examiner	Dr. Muhammad Rehan	PIEAS, Isl
(b)	Internal Examiner	Dr. Noor Muhammad Khan	CUST, Isl
(c)	Supervisor	Dr. Muhammad Ashraf	CUST, Isl

Dr. Muhammad Ashraf
Thesis Supervisor
April, 2019

Dr. Noor Muhammad Khan
Head
Dept. of Electrical Engineering
April, 2019

Dr. Imtiaz Ahmed Taj
Dean
Faculty of Engineering
April, 2019

Author's Declaration

I, **Waqas Ahmed Toor** hereby state that my MS thesis titled "**Study and Simulations of Klystron Modulator Pulse Transformer**" is my own work and has not been submitted previously by me for taking any degree from Capital University of Science and Technology, Islamabad or anywhere else in the country/abroad.

At any time if my statement is found to be incorrect even after my graduation, the University has the right to withdraw my MS Degree.

(Waqas Ahmed Toor)

Registration No: MEE161019

Plagiarism Undertaking

I solemnly declare that research work presented in this thesis titled "*Study and Simulations of Klystron Modulator Pulse Transformer*" is solely my research work with no significant contribution from any other person. Small contribution/help wherever taken has been dully acknowledged and that complete thesis has been written by me.

I understand the zero tolerance policy of the HEC and Capital University of Science and Technology towards plagiarism. Therefore, I as an author of the above titled thesis declare that no portion of my thesis has been plagiarized and any material used as reference is properly referred/cited.

I undertake that if I am found guilty of any formal plagiarism in the above titled thesis even after award of MS Degree, the University reserves the right to withdraw/revoke my MS degree and that HEC and the University have the right to publish my name on the HEC/University website on which names of students are placed who submitted plagiarized work.

(Waqas Ahmed Toor)

Registration No: MEE161019

Acknowledgements

I acknowledge Pakistan Atomice Energy Commision (PAEC), Higher Education Commision (HEC) Pakistan and Capital University of Science and Technology (CUST) for their support and funding to carryout this research work. I am very thankful to my Supervisor Dr. Muhammad Ashrad for his able guidance throughout this research work.

Abstract

Pulse transformer transients are among the most common problems faced, during pulse modulator design. In order to deal with these problems, Pulse transformer's parasitic elements must be minimized during pulse transformer designing. This work contributes towards evaluating parasitic elements i-e distributed capacitance and leakage inductance of Pulse Transformer before construction for more accurate dimensioning of Pulse transformer to achieve desired pulse specifications. Two approaches are adapted to evaluate Pulse transformer parasitic elements. The first one is Analytical approach and the second one is FEMM simulations. In analytical method, pulse transformer cross section in 2D is divided into six regions. Electrical and magnetic energies expressions are derived assuming some approximations in shapes of regions. Electrical energies of different regions of pulse transformer found are multiplied by corresponding depths, depending on dimensions of pulse transformer. Distributed capacitance is evaluated by the electrical energies found. The second approach is 2D finite element method simulations, carried out on FEMM software. For electrical energies same regions as in analytical method, are simulated in FEMM. Modeling of secondary funnel winding in FEMM is done by split conductor. Number of conductors is equal to number of secondary winding turns. Voltage assigned to each conductor is gradually increased from zero to full scale output voltage. With the said modeling more precise electrical energy is calculated to have better estimate of distributed capacitance. For Leakage inductance evaluation, the whole pulse transformer cross section is simulated in magneto static mode. The magnetic energy associated with region in between secondary and primary winding is primarily responsible for leakage inductance. The post processing is done to evaluate distributed capacitance and leakage inductance from electric and magnetic energies respectively. Pulse transformer response to different values of parasitic elements is simulated and analyzed using IEEE standard equivalent circuit for Pulse Transformer. Klystron is a nonlinear load, whose impedance varies with the operating voltage. Klystron manufacturer provides pulse specification requirement for its stable operation. An excessive overshoot can cause arcing in Klystron gun making its life shorter. Variation in voltage at pulse flat top causes

change in phase of microwave produced. In high energy physics experiments, change in microwave power phase results in outside detector collisions in collider applications and experiment results are lost. Similarly an excessive undershoot will damage klystron and measuring equipment on waveguide assembly as klystron is a unidirectional load. Klystron Modulators are designed to meet pulse parameters specifications like rise-time, flat top stability, voltage droop and tail for stable and efficient operation of Klystrons. Pulse transformer parasitic elements play a crucial role in meeting the desired pulse specifications. In this thesis analytical modeling of leakage inductance and parasitic capacitance for three winding topologies are compared considering space between primary and secondary windings. The best one topology having least product of leakage inductance and distributed capacitance is further explored for detail analysis, considering all the regions inside pulse transformer. Finite element method (FEM) simulations are carried out of Funnel winding pulse transformer in FEMM software for more accurate dimensioning of pulse transformer. Finally Pulse transformer core is studied and DC core reset is described with choke designing for efficient utilization of Core cross section area in pulsed operation

Contents

List of Figures

List of Tables

Abbreviations

CERN	European Centre for Nuclear Research
LINAC	Linear Accelerators
FEM	Finite Element Method
FEMM	Finite Element Method Megnetics
HEC	Higher Education Commision
PAEC	Pakistan Atomic Energy Commision
CUST	Capital University of Science and Technology
IEEE	Institute of Electrical and Electronics Engineering

Symbols

L_σ	Leakage Inductance
C_d	Distributed Capacitance
L_{mag}	Magnetizing Inductance
δ	Air-gap length
N_{prim}	Primary Winding Number of Turns
N_{sec}	Secondary Winding Number of Turns
μ_o	Permeability of Free Space
μ_r	Relative Permeability
ϵ_o	Permeability of Free Space
ϵ_{oil}	Permeability of Transformer Oil
ϵ_{iso}	Permeability of winding isolation thickness
T_p	Pulse Duration

Chapter 1

Introduction

1.1 Motivation

High voltage pulse modulator provides the required pulses to drive Klystron, a high power microwave source. Klystron pulse modulator design challenges are meeting the pulse specifications for klystron for particular application. In particle accelerator, change in frequency, phase or amplitude of microwave power affects the beam quality. Microwave power's amplitude, phase and frequency are affected by variation in pulse parameters [1], so there are tight constraints on HV pulse parameters. Usually the pulse transformer is at the output stage of Klystron modulators. In real world pulse transformer's output pulse is not ideal rectangular pulse, even if we assume an ideal rectangular pulse at the input of pulse transformer. The change in shape of input pulse depends on distributed capacitance and leakage inductance of the pulse transformer. The present thesis focus on evaluation of parasitic elements i-e distributed capacitance and leakage inductance of pulse transformer to accurately dimension the pulse transformer. Pulse parameters like rise time, overshoot, flat top ripple and tale are dependent on pulse transformer parasitic. Therefore in designing stage of pulse transformer evaluation of parasitic elements for accurate dimensioning plays a crucial role to achieve the desired pulse specifications. The main objective of this thesis is to evaluate

parasitic elements of pulse transformer before construction. Pulse transformer's response to different values of parasitic elements is also simulated and analyzed using IEEE standard equivalent circuit for pulse transformer, which highlights the importance of parasitic elements in achieving desired pulse specifications.

1.2 Background

This thesis focuses on High voltage pulse transformer for Klystron modulators. High voltage pulse power has a broad field of applications such as particle accelerators, Radars, medical science and industry [2]. Vacuum tubes like Klystron and Magnetron are operated at very high voltages, from few tens of kilo volts to several hundreds of kilo volts and pulse width from few miliseconds to microseconds. HV pulse power supplies used to drive high power pulsed Klystrons and Magnetrons are called pulse modulators. Pulse modulator transfers energy from system input to the output load for a short span of time called pulse width and then power transmission is interrupted for a certain period depending on the pulse repetition rate.

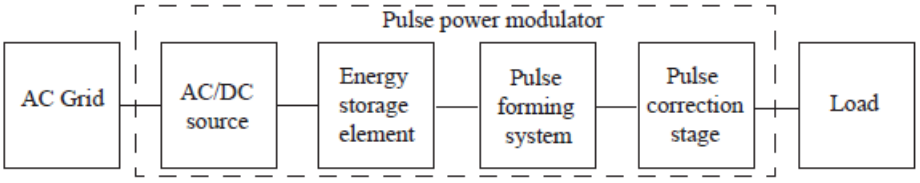

FIGURE 1.1: Pulse modulator structure

General structure of a pulse modulator is shown in Fig. 1.1. The modulator is connected to the AC grid. Usually power drawn from the grid is made constant. Since energy transferred to the load is very high than energy drawn from the grid but for very short span of time therefore an energy storage element is used in between the pulse forming module and the grid. Usually capacitors are used as energy storage element and AC/DC converters are used from grid to these capacitor for desired task.To make constant flow of energy large capacitor banks are

required to avoid voltage droop OR some voltage droop compensation techniques are applied [3].

1.3 Pulse Modulator Topologies

Pulse power modulators have broad range of applications. Different topologies have been developed offering range of energy, repetition rate and pulse width. In the following subsections, three of the modulator topologies for Klystron load are discussed.

1. Line Type modulator
2. Marx Generator
3. Pulse Transformer based modulator

1.3.1 Line Type Modulator

In Pulse forming line (PFL) type modulator, transmission line parasitic elements are used as shown in Fig 1..2 a). The characteristic impedance of transmission line is equal to the load impedance [4]. Since transmission line parasitic per unit length are limited so usually Nanosecond pulses are be produced by PFL-type modulators [2]. For large pulse widths the transmission line model is implemented by combination of capacitors and inductors in pulse forming network (PFN) as shown in Fig. 1.2 b). The size limitation of PFL type modulator is overcome by using PFN in place of transmission line. Using this technique Pulse width of 100us is achievable [5]. Flat top ripple is a challenge in this type of modulator. Resonances of individual components in PFN are studied. For ideal rectangular pulse infinite number of harmonics required, which would result in infinite number of elements in PFN. In order to address this issue either switched converter is used or inductors at different stages of PFN are coupled [6].

In PFN type modulator each element is exposed to the entire output voltage so its voltage is limited to 15-20KV. To overcome this limitation PFN is coupled with pulse transformer or Marx generator.

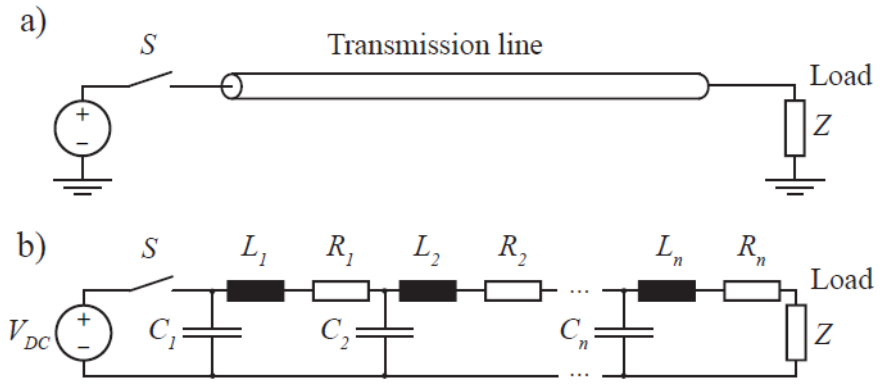

FIGURE 1.2: a) Pulse Forming Line type modulator and b) Pulse Forming Network (PFN) type modulator

1.3.2 Marx Generator

Marx topology is used for very broad Range of pulse power systems. In marx generator several capacitors are charged in parallel and by switches these capacitors are connected in series and a pulse voltage of large amplitude equal to sum of all the capacitors voltages appears at the load. In Fig. 1.3 a three cell marx generator is described. During charging switches S11,S12 and S13 are open and remaining switches are closed so all the three capacitors are charged to the supply voltage V_{charge}. For pulse time all the switches which are closed for charging are now open and S11,S12 and S13 are closed so a pulse voltage equal to 3 Vcharge appear across the load.

The advantage of this topology is that each switch withstands only supply voltage as long as ground isolation is ensured [7]. Initially marx generator were build using spark gap as switches but later on solid state switches replaced spark gap as they are more reliable and with solid state switches the capacitors are not discharged completely which gives better controllability of output pulse.

In marx generator topology challenges are pulse flat top droop, maintenance as all the cells will be dip in oil tank, fault sensing and control as if one cell is faulty the other cells still working. Since pulse length is limited due to voltage droop because of capacitor discharge this problem can be overcome by successive activation of cells. Regular cell activation during the pulse will cause more ripple at the flat

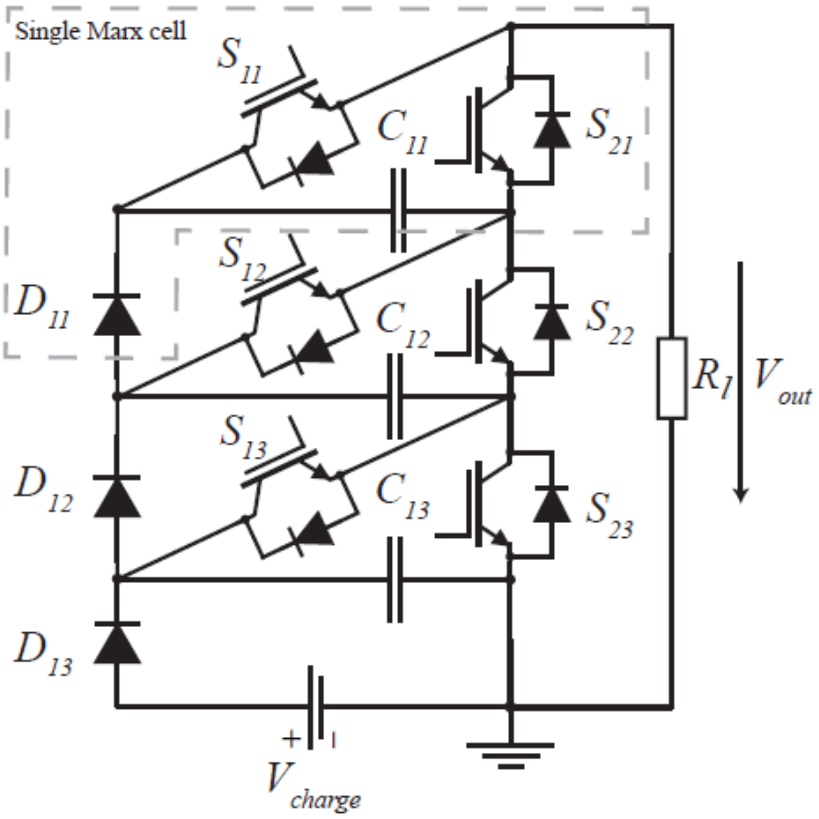

FIGURE 1.3: Three cells Marx Generator

top of pulse. Special correction cells are designed which either have lower charging voltage or modulate their output voltage by switching operations [8].

1.3.3 Pulse Transformer Based Modulator

Pulse transformers used to step up pulse voltages, giving the advantage of low voltage energy storage and switches. Pulse transformer inherent leakage inductance increases the rise time of pulse, so the pulse width must be in microseconds or higher for efficient energy transfer [6]. Core losses also make this topology less efficient [9]. Due to unipolar pulse voltage transformer core has flux swing in one direction only, so often a core reset circuit is used to fully utilize the core. Pulse Transformer design to meet required pulse parameter is a key issue in this modulator topology. Core selection, winding design to reduce parasitic capacitance and

leakage inductance and impedance matching of klystron load to pulse supply are major design challenges [10, 11].

1.4 Choice of Modulator Topology

If Pulse width is in μsec range then PFL type modulators are not feasible,since those are feasible for nsec range pulse widths. If flat top ripple requirement is very strict than PFN type modulators are not feasible, since they have limited number of harmonics causing significant flat top ripple.

For very reliable operation mean time between fault $MTBF > 100000h$ [11], spark gap technology for any of the modulator topology is not feasible. In that case solid state switch based modulators are preferred. since single solid state switch would have isolation problems so Marx generator or Pulse transformer based topology would be feasible.

If low inductance Marx cell is designed it has an advantage of very small Pulse rise time to make this topology very efficient. But small leakage inductance is only advantageous if it is matched with distributed capacitance. In Fig. 1.4 pulse transformer equivalent circuit for the Pulse rising edge is shown. Magnetizing inductance and copper losses are neglected in this circuit diagram. The damping coefficient for this circuit is given by Bortis et al [12]

$$d = \frac{1}{2R_l}\sqrt{\frac{L_\sigma}{C_d}}. \tag{1.1}$$

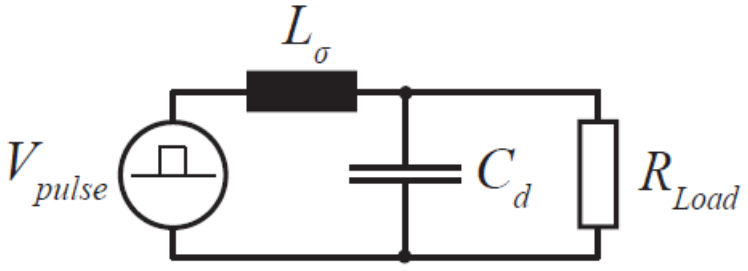

FIGURE 1.4: Simplified pulse Transfomer equivalent During Pulse rise time

To avoid overshoot and settling time problem a sufficient damping $d \approx 1$ is required. For d=1

$$L_\sigma = 4R_l^2 C_d. \tag{1.2}$$

output voltage is given by

$$V(t) = V_p - V_p(1 + \frac{t}{T})e^{-\frac{t}{T}}. \tag{1.3}$$

where,Time constant T is given by

$$T = \sqrt{L_\sigma C_d}. \tag{1.4}$$

Flat top time begins when output voltage reaches the defined flat top band ($V = 1 - 0.5FTS$). Settling time to reach the flat top is one of the required specs, so combination of $L_\sigma and C_d$ can be determined to meet the required specification of Flat top stability.The following relation is obtained by solving above equations.

$$\frac{FTS}{2} = (1 + \frac{t_{settle}}{\sqrt{C_d}2R_l})exp(-\frac{t_{settle}}{\sqrt{C_d}2R_l}). \tag{1.5}$$

Solving the above equation for 8 microsecond settling time 140 μsec flat top length, 0.85% FTS and 883 ohm load will result $C_{d,max} = 470pF$ and$L_{\sigma,max} = 2347\mu H$. As the leakage inductance is in mH range, so an external inductor would be required in case of Marx generator for sufficient damping. While in case of Pulse modulator based topology leakage inductance can easily be increased by just increasing number of turns with having the advantage of greater magnetizing inductance offering lower voltage droop [13].

1.5 Klystrons

Klystron is an RF generator or amplifier. It was invented in 1937 by Varian brothers. It is a vacuum tube in which electron beam accelerated by high potential and modulated by a low power RF signal.Low power RF signal is amplified and

TABLE 1.1: Thales TH801 Klystron's Electrical Data

Parameter	**Value**
Cathode voltage	117 kV
Beam current	131 A
μPerveance	3.27
Electrical resistance	893 Ω at 117 kV
Maximum RF peak power	10 MW
Electrical power	15.33 MW
Electrical pulse duration	1.54 ms (1.7 ms max)
RF pulse duration	1.34 ms
Repetition rate	10 Hz
Efficiency	65%
RF average power	150 kW
Average electrical power	280 kW

transmitted to the waveguide. Electrical data for a commercial Klystron TH801 is given in Table 1.1. For the Pulse modulator, klystron has the following load characteristics

$$I = KV^{3/2}. \tag{1.6}$$

where, I= Klystron current

V=Klystron voltage

K= μPerviance of Klystron

μPerviance is a klystron parameter, determined by the structure of Klystron. It also varies with the aging of Klystron [14]. Fig. 1.5 shows Klystron currrent as a function of Klystron voltage. For simulation purpose Klystron can be modeled as

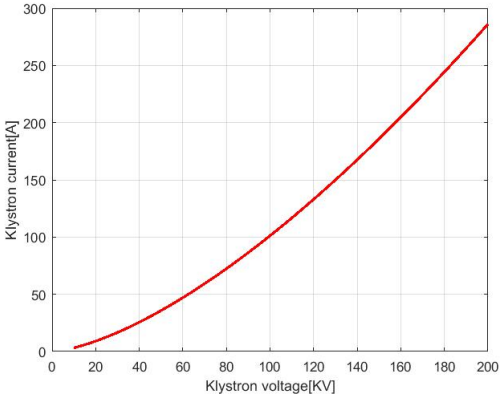

FIGURE 1.5: Klystron Current as a function of Voltage

a diode in series with a Resistor [15] but resistor value must be chosen according to the applied voltage as shown in Fig. 1.6.

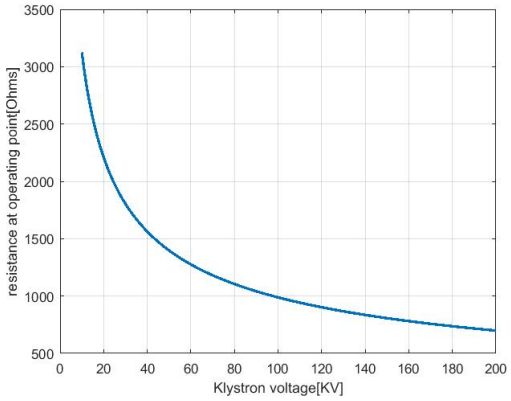

FIGURE 1.6: Klystron Equivalent Resistance as function of Voltage

The beam and RF power of the Klystron are approximately related by

$$P_{Beam} = KV^{5/2}. \tag{1.7}$$

$$P_{RF} = \eta P_{Beam}. \tag{1.8}$$

where, η represents efficiency of the Klystron.

1.5.1 Working Principal of Klystron

Klystron is vacuum device in which electron beam is accelerated from electron gun to the anode. A pencil like beam enters in a buncher cavity where it is modulated by an RF signal. The electron bunches are velocity modulated and travel through the cavity with high kinetic energy due to high potential applied as shown in Fig. 1.7. All the Klystron cavities are tuned nearly to the input signal frequency. When these bunches arrived in the catcher cavity, they given their energy in the form of RF signal, which travel through a vacuum waveguide to a matched load. In particle accelerators this match load is accelerator cavity, which is connected to the waveguide via coupler and waveguide window.Waveguide window separate the high vacuum in the accelerator cavity from pressurized SF_6 in waveguide. For stable operation of klystron a stable voltage pulse is required [16]. Jitter in the

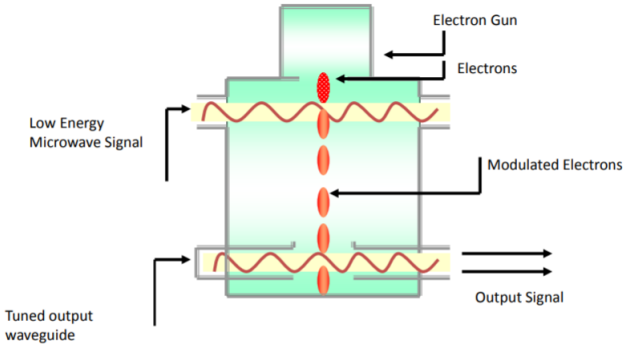

FIGURE 1.7: Klystron working Principal

HV pulse voltage produces jitter in the phase and amplitude of the RF power [17]. For particle accelerator correct phase of RF power is very important. In colliders due to the phase jitters, collision between accelerated particles may occur outside the detector, so useful information is lost for high energy experiments. Low level RF feedback loops correct frequency, phase and impedance problems. Arcing in the gun of Klystron may cause a severe damage to its life. The energy dissipated in klystron arcs must not be greater than 10 to 20 joules for most of the klystrons. Safety interlocks dissipate energy in the current path of klystron to chokes, capacitors or to long transmission lines as soon as the arc occures in klystron [15, 16].

Chapter 2

Literature Review

2.1 Literature Survey

Due to Pulse power applications in a variety of fields, design engineers had to met multiple pulse specification depending on particular application. For predicting output pulse shape and pulse parameters many method to model pulse transformer parasitic are available in literature. Split core pulse transformers are commonly used in modern solid state pulse modulators for medical applications. Chen et al presented theoretical analysis and experimental results of a fraction turn saturable pulse transformer with output voltage range of 19KV for microseconds pulse modulator [18]. Such transformers has dual functions as voltage boosting device and also as magnetic switch. This type of pulse transformer is suitable for surface treatment, corona plasma generation and dielectric barrier discharge applications. The design procedure for leakage inductance of pulse transformer was described by Feifi et al, considering three topologies Conventional parallel winding, asymmetric parallel winding and tapered winding pulse transformers applying 3D FEM software [12]. In many applications high frequency pulse transformers are used in modulators. The design procedure of 100KHz, 115KV isolation voltage pulse transformer is described by Jaritz et al [19]. In Jaritz's work design optimization procedure used high frequency loss calculations with integrated parasitic models

and insulation design. Detail analysis of parasitic elements, considering structure of pulse transformer was done by Bortis et al [20] for solid state microsecond range pulse modulators. In Bortis's work FEM simulations and analytical calculations were carried out for determination of distributed capacitance and leakage inductance for split core pulse transformer, considering two cores.

2.2 Research Gap

To the best of my knowledge, most of the work done to evaluate evaluate leakage inductance is done assuming a constant permeability. In pulse rising edge the operating point on BH-Curve is moving and permeability is not constant. Secondly in rising edge, many high frequency components are present, resulting in different effective core areas for each frequency component. So a set of BH-curve resulting in a set of permeability values for each frequency component is present. More precise evaluation of leakage inductance can be done considering these scenarios.

2.3 Problem Formulation

Pulse transformer distributed capacitance and leakage inductance evaluation for designing of pulse transformer to obtain optimal pulse parameters considering structure of pulse transformer is key objective of this research work. To obtain fast rise time the product of leakage inductance and distributed capacitance must be minimized.

2.4 Research Methodology

Two approaches are adapted to evaluate Pulse transformer parasitic elements. The first one is Analytical approach and the second one is FEMM simulations. In analytical method, pulse transformer cross section in 2D is divided into six

regions. Electrical and magnetic energies expressions are derived assuming some approximations in shapes of regions.Electrical energies found in different regions are then multiplied by corresponding depths, depending on dimensions of pulse transformer. Distributed capacitance is evaluated by the electrical energies found. The second approach is 2D finite element method simulations, carried out o FEMM software. For electrical energies same regions as in analytical method, are simulated in FEMM. Modeling of secondary funnel winding in FEMM is done by split conductor. Number of conductors is equal to number of secondary winding turns. Voltage assigned to each conductor is gradually increased from zero to full scale output voltage. With the said modeling more precise electrical energy is calculated to have better estimate of distributed capacitance. For Leakage inductance evaluation, the whole pulse transformer cross section is simulated in magneto static mode. The magnetic energy in region in between secondary and primary winding is primarily responsible for leakage inductance. The post processing is done to evaluate distributed capacitance and leakage inductance from electric and magnetic energies respectively.

2.5 Contribution

The main contribution of this work is evaluation of Distributed capacitance and leakage inductance of pulse transformer to achieve desired pulse parameter for klystron load.

Chapter 3

Theoretical Analysis

3.1 Background

Transformer is a device works on the principle of electromagnetic induction. The magnetic flux generated in the primary coil having N_{pri} turns linked to the secondary coil via a core of high permeability as shown in Fig. 3.1. If the secondary coil has N_{sec} number of turns, secondary and primary voltages are linked by the following equation.

$$V_{sec} = \frac{N_{sec}}{N_{pri}} V_{pri}. \tag{3.1}$$

$$P_{sec} = P_{pri} => I_{sec} = \frac{N_{pri}}{N_{sec}} I_{pri}. \tag{3.2}$$

The transformer has applications in step up/down voltages, Isolation, sign reversal and impedance matching for maximum power transfer to the load. Real or Practical transformer have limitations.

The energy stored in a capacitor is given by

$$E_{elec} = \frac{1}{2} C V^2. \tag{3.3}$$

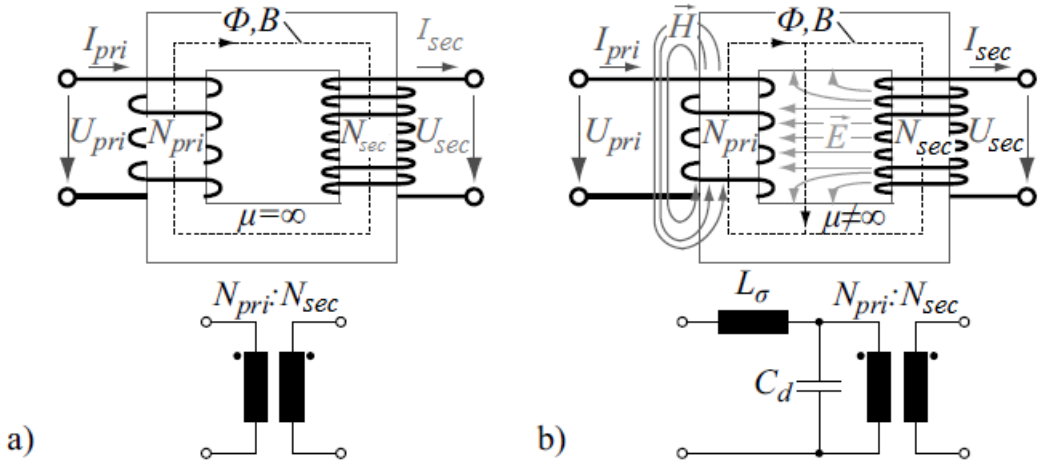

FIGURE 3.1: Pulse Transformer equivalent a)Ideal and b) Real

The energy stored in an inductor is given by

$$E_{mag} = \frac{1}{2}LV^2. \tag{3.4}$$

$$\begin{aligned} E_{elc} &= \frac{1}{2}C_1V_{pri}^2 + \frac{1}{2}C_2V_{sec}^2 + \frac{1}{2}C_{12}(V_{sec} - V_{pri})^2, \\ &= \frac{1}{2}(C_1 + C_{12})V_{pri}^2 + \frac{1}{2}(C_2 + C_{12})V_{sec}^2 - C_{12}V_{pri}V_{sec}. \end{aligned} \tag{3.5}$$

3.2 Pulse Definition

Due to non-ideal behavior of electronic components the pulse produced is not an ideal rectangular pulse. Depending on particular application pulse modulator must meet pulse parameters specifications, like rise time, overshoot, flat top stability, fall time, undershoot, pulse width and repetition rate etc [11]. An ideal and real pulse with parameters are shown in the Fig. 3.2. Pulse parameters are listed as

t_{rise}=Pulse rise time

t_{set}= settling time

t_{flat}=Pulse width

V_{ovs}=Pulse overshoot

FTS=Flat Top stability

t_{fall}=Pulse fall time

t_{reset}=Reset time for Pulse tail

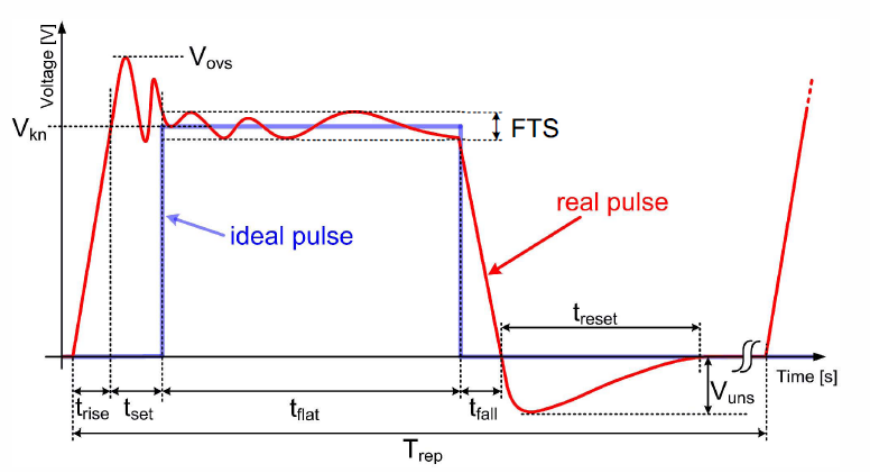

FIGURE 3.2: Real and Ideal pulse with specified parameters

T_{rep}=Pulse repetition time

V_uns=Maximum undershoot

V_{kn}=Pulse voltage

3.3 Pulse Transformer Equivalent Circuit

Pulse transformer transients can be divided into three parts rising edge, flat top and falling edge. The IEEE equivalent circuit for Pulse Transformer is shown in Fig. 3.3 [21]. This circuit can be modified for different regions of pulse, discussed in the following subsections.

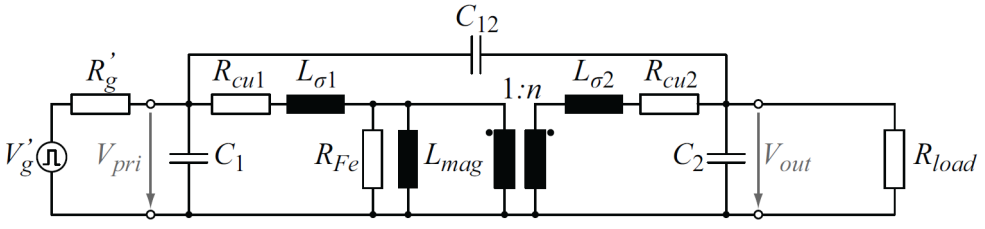

FIGURE 3.3: IEEE Pulse Transformer Equivalent Circuit

wherer, R_{cu1} = Primary winding Resistance

$L_{\sigma 1}$ = Primary winding Leakage Inductance

R_{Cu2} = Secondary winding Resistance

$L_{\sigma 2}$ = Secondary winding Leakage Inductance

C_{12} = Inter-winding Capacitance

C_1 = Primary winding Capacitance

C_2 = Secondary winding Capacitance

R_g = Pulse generator output impedance

R_{load} = Load impedance

R_{Fe} = Represents Core Losses

3.3.1 Pulse Rising Edge

Leading edge of the pulse contains higher frequency components so the equivalent circuit model of the Pulse Transformer can be reduced to Fig. 3.4. Due to very high frequency components in the leading edge, L_{mag} and R_{Fe} are neglected, since at these frequencies impedance of magnetizing inductance and R_{Fe} will be much higher than impedance of leakage inductance and distributed capacitance [21, 22]. The ideal transformer is also ignored as output voltage V_o is simply multiplied with turn ration "n" to get the actual response. In Laplace domain the output voltage V_o is given by

$$V_o(s) = \frac{V_g}{s} \frac{R_{load} || \frac{1}{sC_d}}{R_{load} || \frac{1}{sC_d} + R_g + sL_\sigma}. \tag{3.6}$$

If we consider ideal input pulse (i-e ignoring switching time of IGBT or other high voltage switch),the time domain response of this transfer function for different values of leakage inductance L_σ is obtained using MATLAB shown in Fig. 3.5. Simulation results clearly shows that faster rise time is achieved at lower values of L_σ, keeping C_d constant.

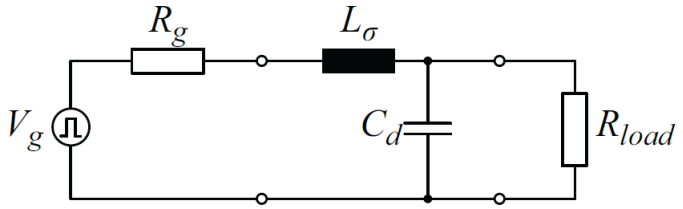

FIGURE 3.4: Simplified Pulse Transformer Equivalent Circuit for Rising edge

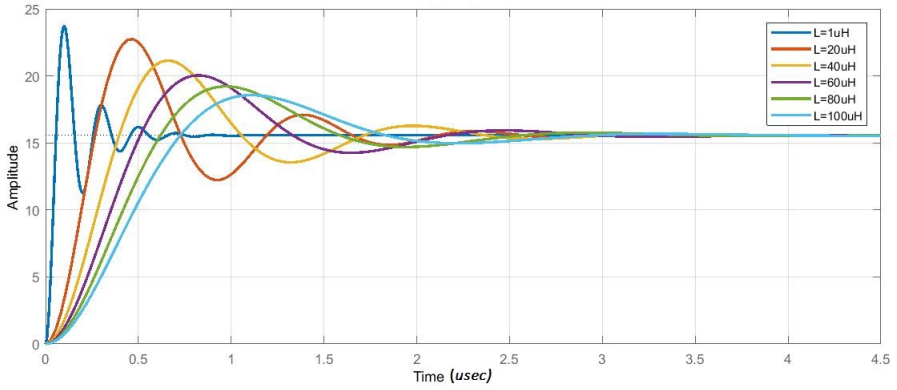

FIGURE 3.5: Pulse Transformer Rising-edge response for variation of leakage inductance

3.3.2 Pulse Flat Top

For flat top response, lower-frequency components are considered. The impedance value of series leakage inductance is very low and shunt capacitance impedance become very high so these are neglected. Only magnetizing inductance is considered [13]. Pulse transformer equivalent circuit for the flat top response is given in the Fig. 3.6 [21].

$$V_o(s) = \frac{V_g}{s} \frac{sL_{mag}||R_{load}}{sL_{mag}||R_{load} + R_g}. \tag{3.7}$$

$$v_o(t) = naV_g exp^{(\frac{-Rt}{L_{mag}})}. \tag{3.8}$$

Where, $a = \dfrac{R_{load}}{R_g + R_{load}}$ and $R = \dfrac{R_g R_{load}}{R_g + R_{load}}$.
The output voltage droop $'D'$ in pulse duration $'t_p'$ is given by

$$D = naV_g\big[1 - exp^{\frac{(-Rt_p)}{L_{mag}}}\big]. \tag{3.9}$$

The voltage droop is exponential and it depends on transformer turn ratio, magnetizing inductance,source/load impedance and the pulse duration [3]. Usually pulse duration is very small so that core is not saturated otherwise voltage droop would be catastrophic. Variation in voltage amplitude during pulse duration for different values of magnetizing inductance L_{mag} is obtained using MATLAB and shown in

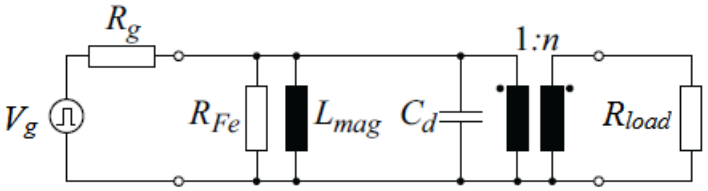

FIGURE 3.6: Pulse Transformer Equivalent Circuit for Flat Top

Fig. 3.7. Result shows larger voltage droop for lower values of magnetizing inductance. So to achieve lower values of voltage droop magnetizing inductance must be kept high and on the same time keeping leakage inductance to lower values for fast pulse rise time.

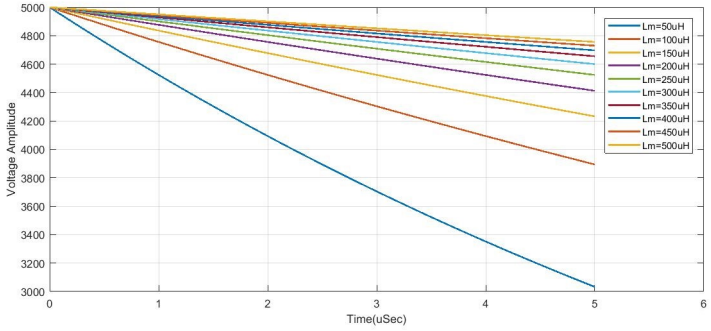

FIGURE 3.7: Pulse Transformer voltage droop during Flat Top for different magnetizing inductance L_{mag}

3.3.3 Pulse Falling Edge

The equivalent circuit of Pulse transformer for trailing edge response is given in Fig. 3.8. Determining the trailing edge response of pulse transformer is little bit more difficult due to the energy stored in the stray capacitance C_d of the transformer and the current flowing through primary winding magnetizing inductance L_{mag} during the trailing edge of the pulse. The generator is removed from the equivalent circuit and the energy stored in the stray elements served as the initial conditions and represented by voltage and current sources. The current source of magnitude equal to current flowing in the magnetizing inductance at the end of pulse $i_m(t_p)$ and the charge stored in the stray capacitance is represented by a step voltage source of magnitude V_l .which is the voltage at the end of pulse on load.

If voltage droop is not considered then load voltage at the end of Pulse would be

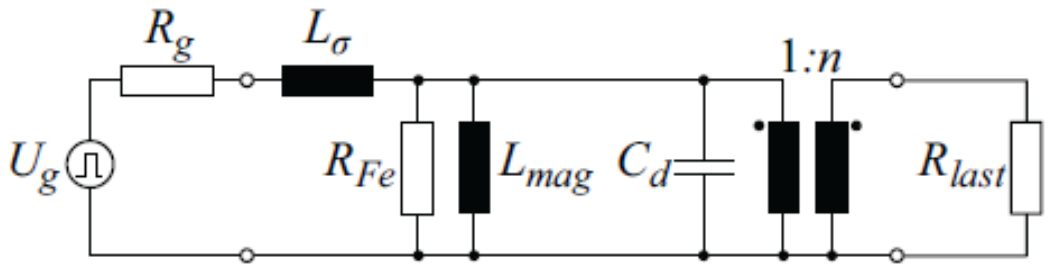

FIGURE 3.8: Pulse Transformer Equivalent Circuit for Pulse Falling edge

$V_l \approx naV_g$ and voltage across $R = R_g||R_{load}$ is given by

$$V_o(s) = \frac{V_l}{s}\frac{sL_{mag}||R}{sL_p||R + \frac{1}{sC_d}} - V_l t_p \frac{\frac{1}{sC_d}||R}{\frac{1}{sC_d}||R + sL_{mag}}. \tag{3.10}$$

$$v_o(t) = \frac{V_l}{\beta_2 - \beta_1}\left[(\beta_2 + \frac{t_p}{L_{mag}C_d})exp^{-\beta_2 t} - (\beta_1 + \frac{t_p}{L_{mag}C_d})exp^{-\beta_1 t}\right]. \tag{3.11}$$

where, $\beta_1, \beta_2 = \left[\frac{1}{2RC_d} \pm \sqrt{(\frac{1}{2RC_d})^2 - \frac{1}{L_{mag}C_d}}\right] = \gamma\left[1 \pm \sqrt{1 - \frac{1}{k^2}}\right]$.

$'k'$ is called damping factor or constant. The trailing edge response of pulse transformer for different values of damping factor $k = \frac{1}{2R}\sqrt{\frac{L_{mag}}{C_d}}$ is obtained using MATLAB shown in Fig. 3.9.

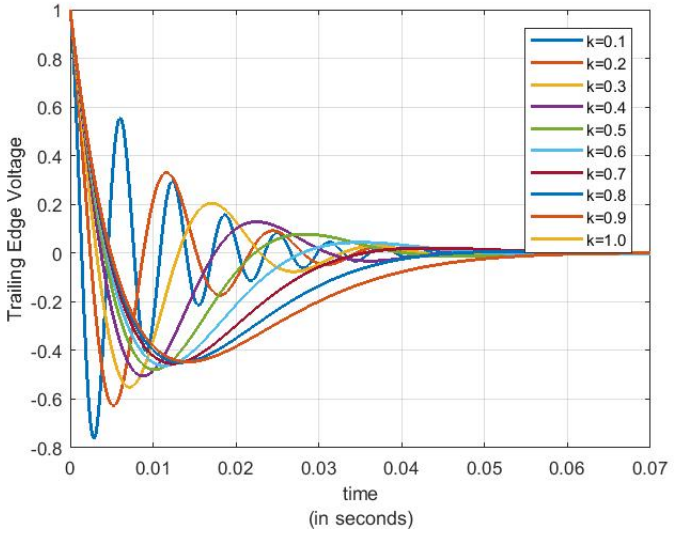

FIGURE 3.9: Pulse Transformer Trailing-edge Response for variation of damping coefficient 'k'

3.4 Winding Topology

Three types of winding topologies are discussed on the basis of the $L_\sigma C_d$ product. Where the leakage inductance L_σ is determined by the stored energy in magnetic field H and distributed capacitance C_d is determined by the energy stored in the electric field E [23, 24]. The best one topology would be that which has the lowest value of this product $L_\sigma C_d$.

3.4.1 Parallel Winding

Parallel winding topology is the best known winding type.In this topology both primary and secondary winding are wound on the same core leg over one another. To avoid breakdown a fix distance is maintained between the windings and a material of high permitivity value is used in between, depending on the output voltage of transformer. For low voltages both windings can be nested to reduce leakage inductance. Due to high Pulsed primary current, primary winding is often of many round conductors or wide foil conductor. In general both legs of the transformer core are wound in parallel it reduces the leakage inductance L_σ by half due to parallel circuit but doubles the distributed capacitance C_d, so the product $L_\sigma C_d$ remains constant [25, 26].

Usually Pulse transformer core is grounded and inner winding is low voltage primary winding. Primary winding is wound on a support wrapped directly on the transformer core.To minimize the leakage inductance the entire height of transformer leg is wound by round or foil conductor and to ensure homogeneous current distribution. Due to smaller peak current in the secondary winding, a single layer round conductor may be used. The last turn of the secondary winding is made of a larger diameter pipe, called Guard ring as shown in Fig. 3.10. The purpose of guard ring is to form a homogeneous electric field with respect to primary winding and core and to reduce the resulting field strength [26].It should be noted that the guard ring is separated or remains open at one point to avoid Transformer short circuit.

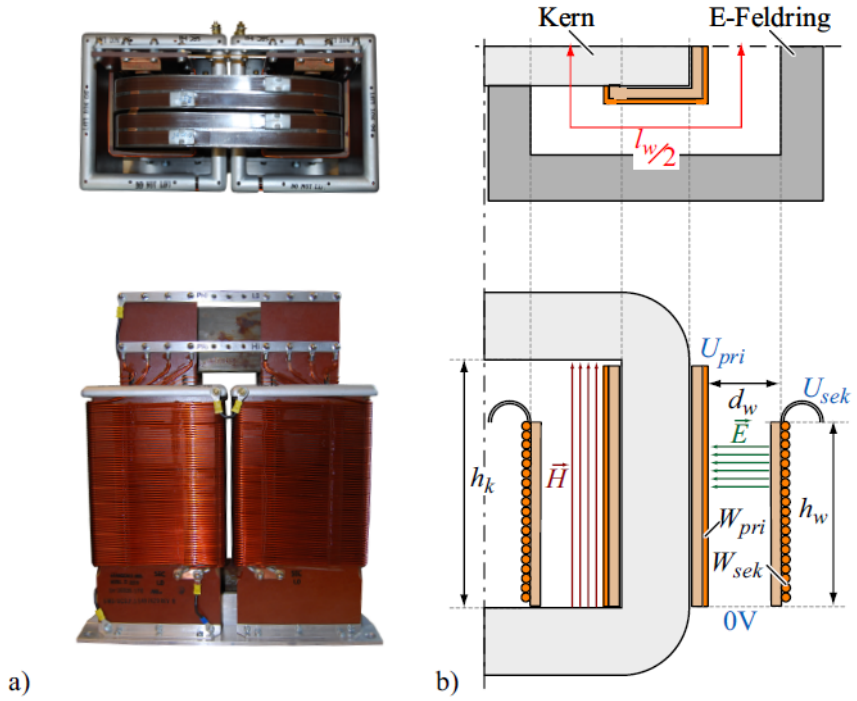

FIGURE 3.10: (a)Top and Front view of Parallel windings Pulse Transformer (b)Sketch of the Cross section of Parallel winding Pulse Transformer

Electrical energy E_{elect} and magnetic energy E_{mag} in space between windings are given by [23]

$$\begin{aligned} E_{elect} &= \frac{1}{2}\epsilon \int_V \vec{E}^2 dV, \\ &= \frac{1}{2} C_d U_{pri}^2. \end{aligned} \tag{3.12}$$

$$\begin{aligned} E_{mag} &= \frac{1}{2}\mu \int_V \vec{H}^2 dV, \\ &= \frac{1}{2} L_\sigma I_{pri}^2. \end{aligned} \tag{3.13}$$

$$\begin{aligned} U_{prim}(y) &= \frac{y}{h_w} U_{prim}, \\ U_{sec}(y) &= \frac{y}{h_w} U_{sec}. \end{aligned} \tag{3.14}$$

The electric field lines in space between primary and secondary winding increases along the core leg height $'y'$, due to the voltage gradient between primary and secondary winding.Consequently the electric field $\vec{E}$ can be determined as a function

of y and turn ratio $n = \frac{N_{sec}}{N_{prim}}$.

$$\Delta U(y) = \int_0^{d_w} \vec{E}(y) dx. \tag{3.15}$$

$$\begin{aligned} |\vec{E}(y)| &= \frac{\Delta U(y)}{d_w}, \\ &= \frac{U_{sec}(y) - U_{pri}(y)}{d_w}, \\ &= \frac{U_{pri}(n-1)y}{h_w d_w}. \end{aligned} \tag{3.16}$$

The electrical energy between two windings and distributed capacitance for one leg, assuming a homogeneous structure with medium circumference l_w can be determined as

$$\begin{aligned} E_{elect} &= \frac{1}{2}\epsilon \int_V \vec{E}(y)^2 dV, \\ &= \frac{1}{2}\epsilon \int_0^{l_w} \int_0^{h_w} \int_0^{d_w} (\frac{U_{sec} y}{h_w d_w})^2 dx dy dz, \\ &= \frac{1}{6}\epsilon U_{sec}^2 (\frac{l_w h_w}{d_w}) = \frac{1}{2} C_d U_{pri}^2. \end{aligned} \tag{3.17}$$

$$C_d = \frac{1}{3}\epsilon n^2 (\frac{l_w h_w}{d_w}). \tag{3.18}$$

The leakage inductance L_σ can be determined in the same way as the distributed capacitance C_d between primary and secondary windings. Again the round conductors are replaced by rectangular strip conductors of the same size, assuming homogeneous current distribution.

$$N_{prim} I_{prim} = \oint \vec{H} dl. \tag{3.19}$$

$$|\vec{H}| = \frac{N_{prim} I_{prim}}{h_k}. \tag{3.20}$$

$$\begin{aligned} E_{mag} &= \frac{1}{2}\mu \int_V \vec{H}^2 dV = \frac{1}{2}\mu \int_0^{l_w} \int_0^{h_k} \int_0^{d_w} \left(\frac{N_{prim} I_{prim}}{h_k}\right)^2 dx dy dz, \\ &= \frac{1}{2}\mu \big(N_{prim} I_{prim}\big)^2 \frac{l_w d_w}{h_k} = \frac{1}{2}\mu L_\sigma I_{prim}^2. \end{aligned} \tag{3.21}$$

$$L_\sigma = \mu \frac{N_{prim}^2 l_w d_w}{h_k}. \tag{3.22}$$

If both legs of transformer are considered distributed capacitance would be doubled due to parallel connection and leakage inductance would be half. So the product $L_\sigma C_d$ for one leg of transformer is same as for the whole transformer and parallel connection of winding does no improvement on rise time of the pulse.

$$L_\sigma C_d = \frac{1}{3}\epsilon\mu \frac{N_{sec}^2 l_w^2 h_w}{h_c}. \tag{3.23}$$

3.4.2 Funnel Winding

The full secondary voltage in parallel winding transformer will appear at the upper end only due to linear voltage distribution between primary and secondary windings along the height $'y'$. This clearly shows that insulation distance requirement between both the windings is lesser at the bottom end than the upper end. To make the uniform electric field strength between both the windings, isolation distance can be increased gradually from bottom to top resulting in Funnel shape winding as shown in Fig. 3.11.

Using this technique leakage flux will be reduced as compare to parallel winding transformer due to lesser space between primary and secondary windings. To find distributed capacitanc, electric energy between primary and secondary winding is given by

$$\Delta U(y) = \int_0^{d_w} \vec{E} dx \implies \vec{E} = \frac{\Delta U}{d_w}. \tag{3.24}$$

$$\begin{aligned} E_{elect} &= \frac{1}{2}\epsilon \int_V \vec{E}^2 dV, \\ &= \frac{1}{2}\epsilon \int_0^{l_w} \int_0^{h_w} \int_0^{\frac{h_w}{d_w} y} {\frac{U_{sec}}{d_w}}^2 dxdydz, \\ &= \frac{1}{4}\epsilon U_{sec}^2 \left(\frac{l_w h_w}{d_w}\right) = \frac{1}{2} C_d U_{prim}^2. \end{aligned} \tag{3.25}$$

$$C_d = \frac{1}{2}\epsilon n^2 \left(\frac{l_w h_w}{d_w}\right). \tag{3.26}$$

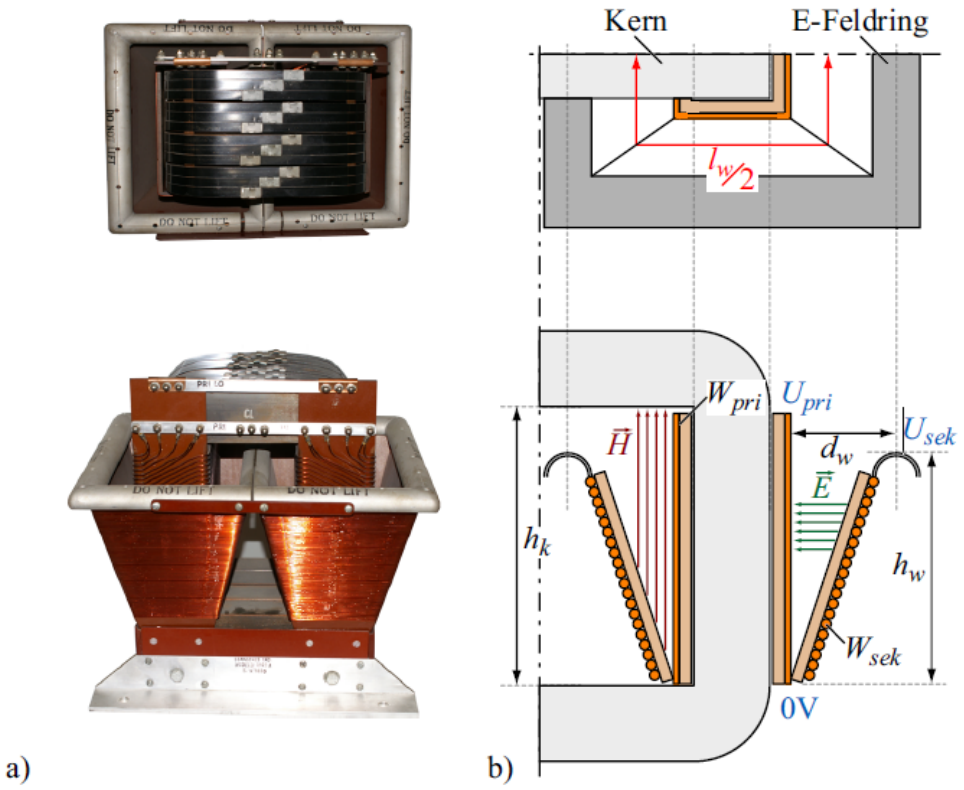

FIGURE 3.11: (a)Top and Front view of Funnel windings Pulse Transformer (b)Sketch of the Cross section of Funnel winding Pulse Transformer

$$|\vec{H}| = \frac{N_{prim} I_{prim}}{h_k}. \tag{3.27}$$

$$\begin{aligned} E_{mag} &= \frac{1}{2}\mu \int_V H^2 dV, \\ &= \frac{1}{2}\mu \int_0^{l_w} \int_0^{h_k} \int_0^{\frac{d_w}{h_w} y} \left(\frac{N_{prim} I_{prim}}{h_k}\right)^2 dx dy dz, \\ &= \frac{1}{4}\mu \left(N_{prim} I_{prim}\right)^2 \frac{l_w d_w}{h_c} = \frac{1}{2} L_\sigma I_{prim}^2. \end{aligned} \tag{3.28}$$

The leakage inductance L_σ and the corresponding $L_\sigma C_d$ product is given by

$$L_\sigma = \frac{1}{2}\mu \frac{N_{prim}^2 l_w d_w}{h_k}. \tag{3.29}$$

$$L_\sigma C_d = \frac{1}{4}\epsilon\mu \frac{N_{sec}^2 l_w^2 h_w}{h_k}. \tag{3.30}$$

By using funnel winding topology the product $L_\sigma C_d$ is reduced by 25% compare to parallel winding topology, this will result in shortening of rise time by 13.4%.

3.4.3 Film Winding

In this winding topology both primary and secondary windings are made of foil conductors. The primary winding is wrapped on a carrier over the core as in other topologies. The secondary winding is wrapped on the same carrier around the primary winding through a thickness d_{iso} of low permeability material for isolation, as shown in Fig. 3.12 . Thickness of insulation foil can be kept small as the voltage difference between two secondary winding turns $U_{w,w}$ is equal to the full scale secondary voltage U_{sec} divided by number secondary turns N_{sec}.

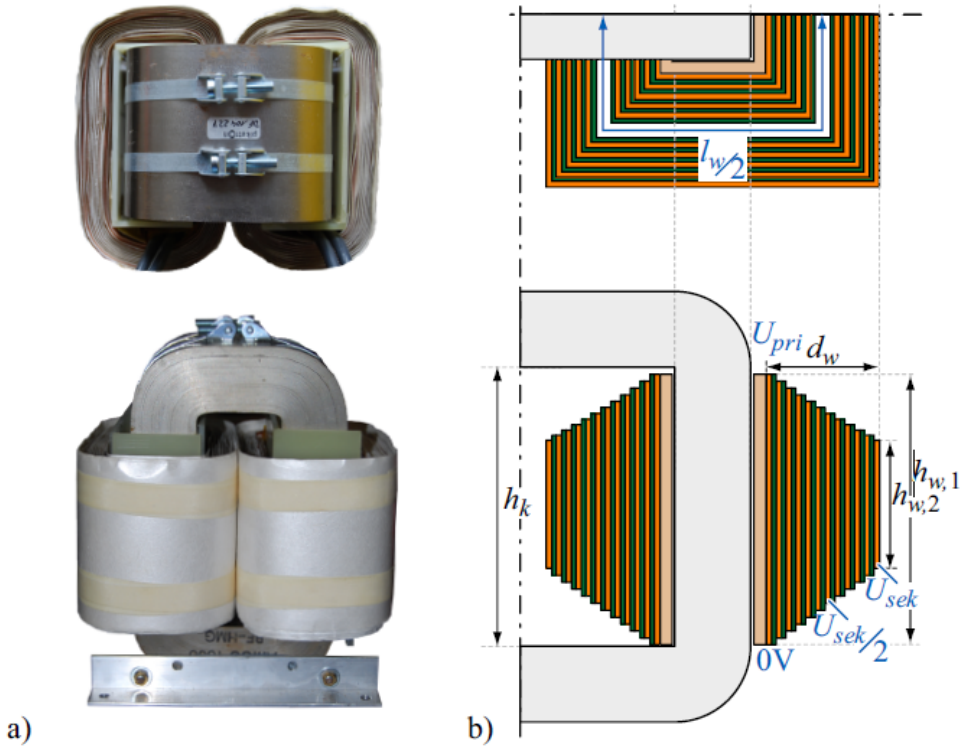

FIGURE 3.12: (a)Top and Front view of Film windings Pulse Transformer (b)Sketch of the Cross section of Film winding Pulse Transformer

$$U_{w,w} = \frac{U_{sec}}{N_{sec}}. \tag{3.31}$$

Since the secondary voltage increases per turn from inner to outer side so the winding film height must be decreased gradually to maintain required isolation distance from the core as shown in the Fig. 3.12. Totall thickness of film winding can be determined from conductor thickness d_{cu}, isolation thickness d_{iso} and

number of secondary turns N_{sec} as

$$d_w = N_{sec}(d_{iso} + d_{cu}). \tag{3.32}$$

The distributed capacitance C_d comprise of series connection of inter turn capacitances $C_{w,w}$ [25]. As the foil height is decreasing from inside to outside, so median height $h_w = \dfrac{h_{w1} + h_{w2}}{2}$ and median winding length l_w are used for approximate distributed capacitance calculations with $k = \frac{d_{cu}}{d_{iso}}$ it is given by

$$d_{\text{iso}} = \frac{d_w}{(k+1)N_{sec}}. \tag{3.33}$$

$$\begin{aligned} C_d &= n^2 \frac{C_{w,w}}{N_{sec}} = \epsilon n^2 \frac{h_w l_w}{d_{iso} N_{sec}}, \\ &= (k+1)\epsilon n^2 \left(\frac{h_w l_w}{d_w} \right). \end{aligned} \tag{3.34}$$

For calculating leakage inductance L_σ of the film transformer homogeneously distributed secondary current I_{sec} in the film winding is assumed.From Ampere's Law magnetic field as a function of secondary winding turns is given by

$$\begin{aligned} \vec{H}(n_L) &= \frac{N_{prim} I_{prim}}{h_k} - \frac{n_L I_{sec}}{h_k}, \\ &= \frac{I_{prim}}{h_k} \left(N_{prim} - \frac{n_L}{n} \right). \end{aligned} \tag{3.35}$$

Sum of all partial magnetic energies is equal to total magnetic energy E_{mag} between all turns.

$$\begin{aligned} E_{mag} &= \frac{1}{2}\mu \sum_{n_L=1}^{N_{sec}} \vec{H}(n_L)^2 V(n_L), \\ &= \frac{1}{2}\mu \sum_{n_L=1}^{N_{sec}} \frac{I_{prim}^2}{h_k^2} (N_{prim} - \frac{n_L}{n})^2 V(n_L), \\ &= \frac{1}{2}\mu \frac{I_{prim}^2 l_w d_w}{N_{sec} h_k} \left(N_{prim}^2 N_{sec} - \frac{2N_{prim}}{n} \sum_{n_L=1}^{N_{sec}} n_L + \frac{1}{n^2} \sum_{n_L=1}^{N_{sec}} n_L^2 \right), \\ &\approx \frac{1}{2}\mu \frac{I_{prim}^2 l_w d_w}{N_{sec} h_k} \left(N_{prim}^2 N_{sec} - N_{prim}^2 N_{sec} + N_{prim}^2 \frac{N_{sec}}{3} \right), \\ E_{mag} &= \frac{1}{6}\mu (N_{prim} I_{prim})^2 \frac{l_w d_w}{h_k} = \frac{1}{2} L_\sigma I_{prim}^2. \end{aligned} \tag{3.36}$$

TABLE 3.1: Comparison of $L_\sigma C_d$ product of three winding toplologies

Winding Topology	$L_\sigma C_d$ product
Parallel Winding	$\frac{1}{3}.\epsilon\mu\frac{N_{sec}^2.l_w^2.h_w}{h_k}$
Funnel Winding	$\frac{1}{4}.\epsilon\mu\frac{N_{sec}^2.l_w^2.h_w}{h_k}$
Film Winding	$\frac{k+1}{3}.\epsilon\mu\frac{N_{sec}^2.l_w^2.h_w}{h_k}$

The determined leakage inductance of Foil winding Pulse Transformer is given as

$$L_\sigma = \frac{1}{3}\mu\frac{N_{prim}^2 l_w d_w}{h_k}. \tag{3.37}$$

The corresponding $L_\sigma C_d$ product is given as

$$L_\sigma C_d = \frac{k+1}{3}\epsilon\mu\frac{N_{sec}^2 l_w^2 h_w}{h_k}. \tag{3.38}$$

3.5 Choice of Winding Topology

For all the three winding topologies discussed, the first approximation is that $L_\sigma C_d$ product is independent of the winding distance d_w. Due to better insulation material or isolation capacity of transformer oil the winding distance d_w can be decreased. By reducing distance d_w winding height h_w may be decreased. It will not improve the rise time for a particular topology but smaller core length resulting in the smaller transformer volume. In Foil winding Pulse transformer the ratio of conductor and insulation thickness $k = \frac{d_{cu}}{d_{iso}} \to 0$, if thickness of conductor is very small($d_{cu} \to 0$). In this condition when $k \approx 0$ the Film winding and Parallel winding will have approximately same value of $L_\sigma C_d$ product value.

The $L_\sigma C_d$ product for the three winding topologies are listed in Table. it is obvious that Funnel winding has the lowest $L_\sigma C_d$ product value and hence the fastest rise time thats why this winding topology is selected in this Research Work. For very

small value of $\frac{d_w}{h_w}$ it can be approximated that

$$\frac{h_w}{h_k} = \frac{h_w}{h_w + d_w} = \frac{1}{1 + \frac{d_w}{h_w}} \approx 1. \tag{3.39}$$

In all the three winding topologies fo $h_w \gg d_w$ the $L_\sigma C_d$ product depends only on the square of winding circumference l_w and number of secondary turns N_{sec}. In addition the two parameters N_{sec} and l_w are related by core cross section area A_k and core material properties. Assuming a square core cross section area and bipolar core operation i-e from $-B_{sat}$ to $+B_{sat}$ the parameters N_{sec} and l_w are related by

$$l_w \approx 4\sqrt{A_k}\,, \qquad N_{sec} = \frac{U_{sec} T_p}{2 B_{sat} A_k}. \tag{3.40}$$

Since U_{sec} and T_p are fixed system parameters so Pulse Rise time T_r depends on N_{sec} and core properties only. For all the three topologies

$$\begin{aligned} L_\sigma C_d \propto (l_w N_{sec})^2 &= \left(4\sqrt{A_k} N_{sec}\right)^2, \\ &= \left(4\sqrt{A_k}\frac{U_{sec} T_p}{2 B_{sat} A_k}\right)^2, \\ &= 4\left(\frac{U_{sec} T_p}{B_{sat}}\right)^2 \frac{1}{A_k}, \\ &= 8\frac{U_{sec} T_p N_{sec}}{B_{sat}}. \end{aligned} \tag{3.41}$$

Equation 2.41 shows that $L_\sigma C_d$ product and hence the pulse rise time depends on secondary number of turns N_{sec} and the core cross section area A_k. To minimize the pulse rise time N_{sec} must be minimized and the core cross section area A_k must be selected according to maximum flux density B_{sat}. In a conventional pulse transformer where primary and secondary windings are wound on a same core the minimum number of primary turns N_{prim} is equal to 1, So by turn ratio the minimum secondary turns are given by

$$N_{sec,\min} = \frac{U_{sec}}{U_{prim}}. \tag{3.42}$$

Since for conventional one core transformer the minimum number of primary turn is 1 so $L_\sigma C_d$ product cannot be shrink further to attain smaller pulse rise time.

To shrink it further Fractional primary turn is possible if multiple cores are used, which are generally known as Fractional turn transformer, split-core, voltage adder or matrix pulse Transformer [27–29].

$$\begin{aligned} A_{k,\min} &= \frac{U_{sec} T_p}{2 B_{sat} N_{sec,\min}}, \\ &= \frac{U_{prim} T_p}{2 B_{sat}}. \end{aligned} \tag{3.43}$$

3.6 Windings Connection Arrangement

Pulse transformer core are usually of U-shape, with both legs wound for high voltage high current applications and one leg wound for low power applications. Pulse Transformer winding arrangements for primary and secondary windings can be series or parallel connections. In this way there are four possibilities as shown in the Fig. 3.13.

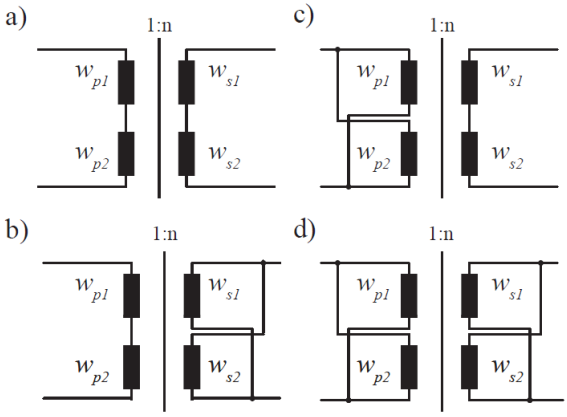

FIGURE 3.13: Series and Parallel winding connections in Pulse Transformer

In (a) and (b) secondary windings are connected in series and parallel respectively and primary windings are in series and. while in (c) and (d) secondary windings are connected in series and parallel respectively and primary windings are in parallel. For ease of analysis single layer windings are considered. Parallel connection of primary windings supports comparatively higher primary current as Pulse transformers are used for stepping up the voltage in Pulse modulators therefore (a) and (b) are not considered. In (c) when using series connection of secondary windings

the second winding will have a floating voltage $V_{sec}/2$ and the number of secondary turns on each winding will be half as compare to parallel connection of secondary windings.This will not reduce the leakage inductance but core window height may be reduced. In (d) the secondary winding is connected in parallel, this will have simple windings construction and lesser insulation requirement inside window, as both winding have common ground at one end as shown in Fig. 3.14. In parallel connection the leakage inductance may become half but its effect is compensated by th doubled parasitic capacitance making the $L_\sigma C_d$ product constant.

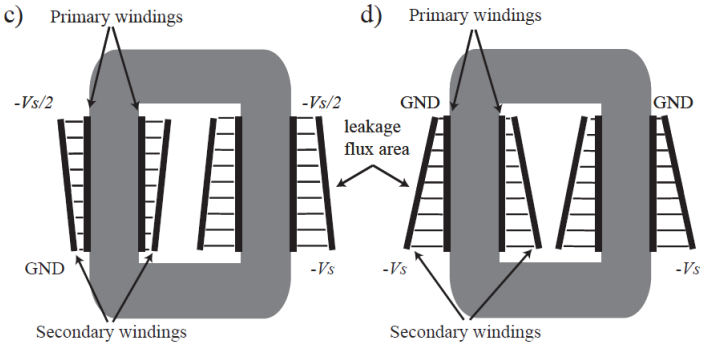

FIGURE 3.14: Winding Structure for (c)Series and (d)Parallel connected Secondary Windings

3.7 Multiple Cores Pulse Transformers

Split core OR fractional turn primary Pulse Transformers contain multiple cores. Each core has its individual primary winding and secondary windings enclose all the cores. For example a half turn primary Pulse Transformer with two cores, is shown in the Fig. 3.15.

Idea of split core transformer originated from classical induction accelerators, where a single turn secondary wire surrounded by "N" magnetic cells. This type of conventional setup provides a voltage step up ratio of N. In split core transformer, if a single turn primary is used with N_1 number of cores and N_2 number of secondary turns then a voltage step up ratio of $N_2 * N_1$ is achieved [28]. Due to very high primary current, each primary winding usually consist of multiple

FIGURE 3.15: Half Turn Primary Pulse Transformer

conductors. Number of HV pulse supplies is equal to number of primary windings. Each pulse supply power all the primary windings through their individual conductors [29] as shown in Fig. 3.16. In this way if a particular pulse supply is switched on little bit delay or switch off little early, sum of all the reamining output voltage will not appear across.It was verified by Crewson et al practically switching off one pulse supply. IGBTs are used instead of thyristors in this topology as IGBTs have controlled turn off characteristic. By varying the pulse width at the gate of IGBT output HV pulse width can be controlled which is possible by software without accessing the modulator hardware itself [30]. This feature is very helpful during conditioning of accelerating cavities. Since PFN are not used in such schemes so there should be compensator circuits for voltage droop caused by the lowering of capacitor voltage due to discharge during the pulse width. In Fig. 3.17, series connection of two transformers and transformer with two cores are presented. The winding length of both the scheme are

$$l_w = 4a_k + 4b_k + 8b_w. \tag{3.44}$$

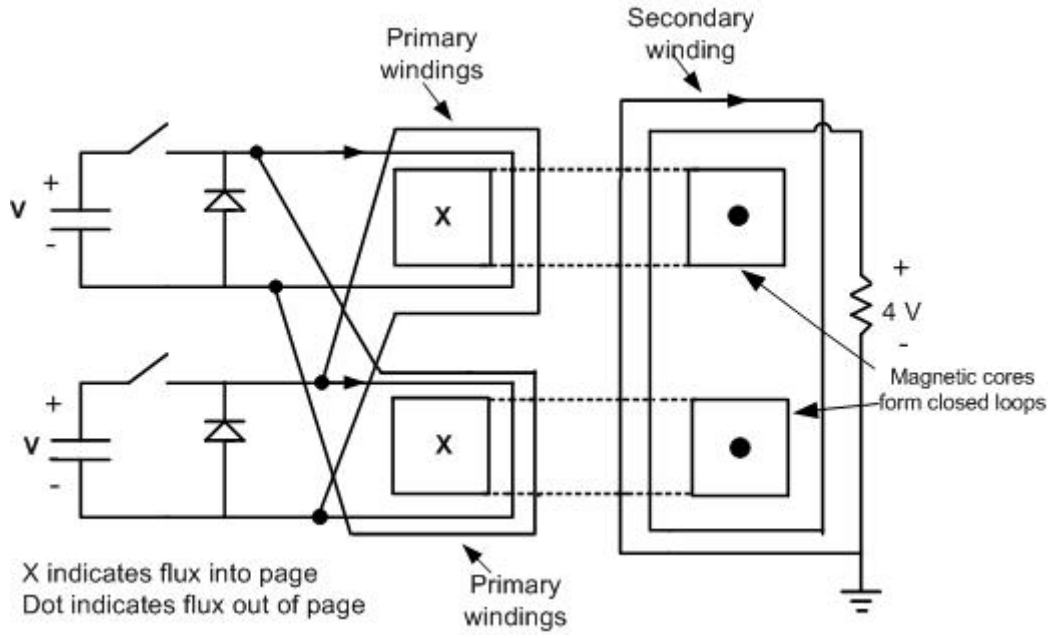

FIGURE 3.16: Half Turn Primary Pulse Transformer with each pulse supply driving both the primary windings through individual conductors.

$$l_w^{'} = 2a_k + 4b_k + 4b_w. \tag{3.45}$$

where, $l_w^{'}$ is winding length of transformer with two cores and l_w is winding length for series connection of two transformer.

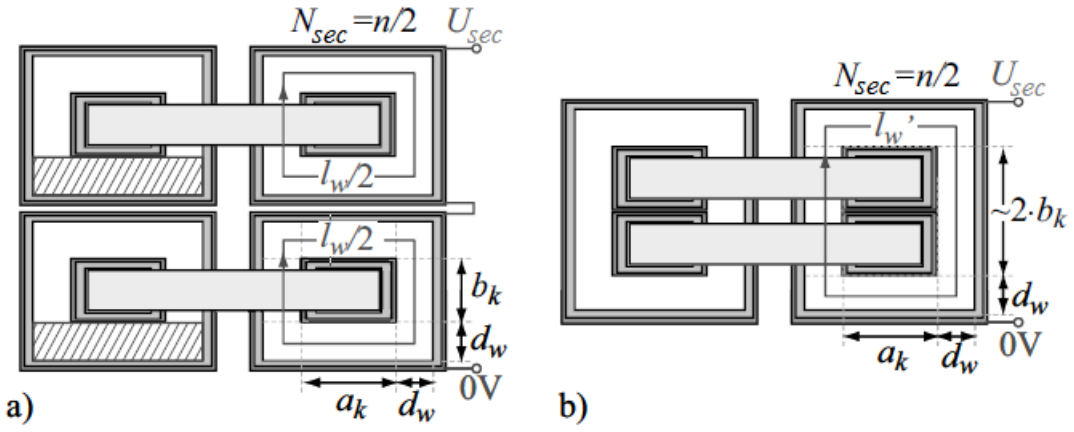

FIGURE 3.17: (a) Series connection of two identical pulse transformer with $N_{sec} = \frac{n}{2}$ and (b) Pulse Transformer with two cores with winding length $l_w^{'}$

Now consider a numerical example to compare above two schemes.In series connection of two transformers or with the transformer having two cores, the secondary

voltage is given by

$$U_{sec} = \frac{d\psi(t)}{dt} = \frac{\phi(t)}{dt} = N_{sec} 2A_k \frac{dB(t)}{dt}. \tag{3.46}$$

For a Pulse Transformer with following data

$U_{sec} = 200kV$

$|E_{max}| = 20kV/mm$ assumed breakdown field strength

$U_{pri} = 1000V$

$T_p = 5\mu sec$

$\Delta B = 2T$

and $N_{pri} = 1$

The winding distance required to avoid breakdown strength would be

$d_w > \frac{U_{sec}}{|E_{max}|} = \frac{200kV}{20kV/mm} = 10mm$

With the safety factor of 2.5, the winding distance $d_w = 25mm$

using Equation 2.40, for $N_{sec} = 100$, as two primaries are there

$A_k = \frac{U_{sec} T_p}{2B_{sat} N_{sec}} = 25cm^2$

For square crossection core, $a_k = b_k = 5cm$ and corresponding secondary winding length for two series connected and two cores pulse transformer are $l_w = 60cm$ and $l_w^{'} = 40cm$ respectively. So 33% of improvement in rise time is achieved by using two core Pulse transformer as compare to two series connected Pulse transformers considering secondary winding lengths only. As the number of cores are increased, further improvement in $L_\sigma C_d$ and hence rise time is achieved. Also the Transformer volume and cost is also increased. Generalized expressions for winding lengths for 'p' series connected Pulse Transformers and a Transformer with 'p'cores are given by

$$l_w = p(2a_k + 2b_k + 4d_w). \tag{3.47}$$

$$l_w^{'} = 2a_k + 2Pb_k + 4d_w. \tag{3.48}$$

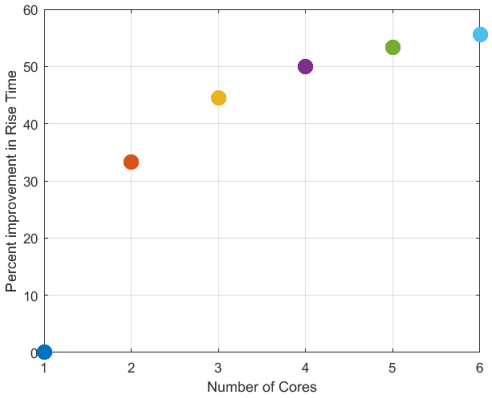

FIGURE 3.18: Percent improvement in $L_\sigma C_d$ OR Pulse rise time due to multiple cores as compare to series connection of multiple Pulse Transformers

For a square core with $ak = b_k = a$ the percent change in winding length or in other words, percent improvement in rise time is plotted in Fig. 3.18 and given by

$$\frac{\Delta l}{l_w} * 100 = \frac{p-1}{2p}\left(\frac{a+2d_w}{a+d_w}\right) * 100$$

3.8 Calculation of Pulse Transformer Parasitic

To achieve specifications on Pulse Rise time the distributed capacitance and leakage inductance must be minimized [22] and for Pulse overshoot specification, they should be in certain relationship depending on the load. So to predict accurately the pulse shape of a pulse transformer, precise calculation of parasitic elements is required. In Section 2.5, the product of distributed capacitance and leakage inductance of different winding topologies were compared and Funnel winding has the smallest $L_\sigma C_d$ product and hence the shortest Pulse rise time.Those results were obtained by considering electrical energy E_{elect} and magnetic energy E_{mag} in the region between primary and secondary windings only. In actual, other regions of pulse transformer, like between windings and core, between winding and tank walls also contribute towards parasitic elements.

3.8.1 Calculation of Distributed Capacitance

To determine distributed capacitance of a funnel winding the electric energy is calculated in different regions of pulse transformer. Pulse transformer cross section is divided into six regionsR_1, R_2, R_3, R_4, R_5 and R_6 [26] as shown in Fig. 3.19.

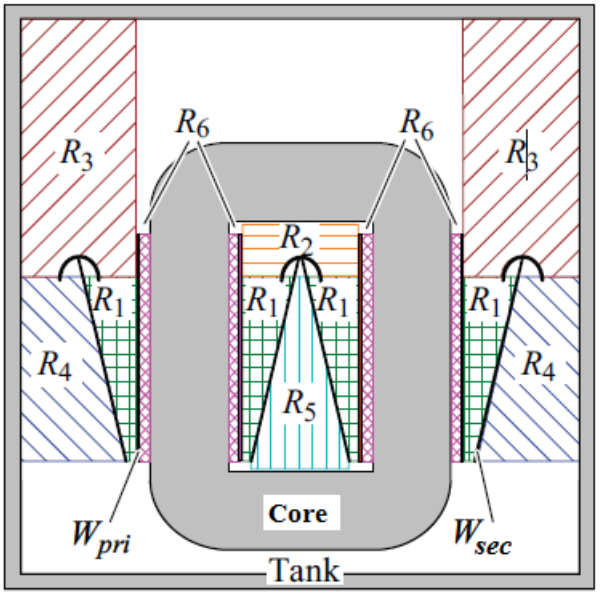

FIGURE 3.19: Sketch of the cross section of Funnel winding Pulse Transformer with areas $R_1 - R_6$

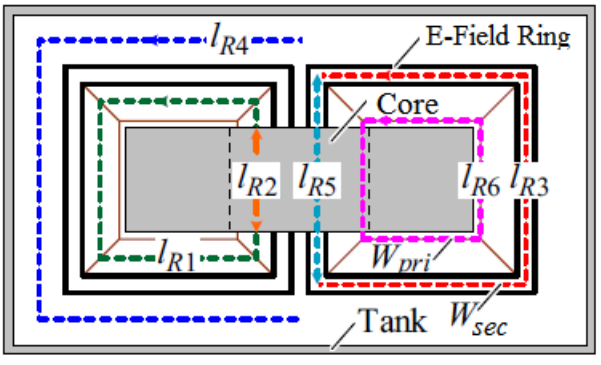

FIGURE 3.20: The corresponding perimeter lengths $l_{R1} - l_{R6}$ for areas $R_1 - R_6$ for calculation of Electrical energy and distributed capacitance C_d

Since the Pulse Transformer shape is symmetric, so to determine distributed energy, each individual calculated energy for areas $R_1 - R_6$ is multiplied by the corresponding perimeter lengths $l_{R1} - l_{R6}$ shown in Fig. 3.20.

Electrical energy for area R_1 has already been determined in section 2.4 for selection of most appropriate winding topology. In this section, in addition the geometry of winding carrier with thickness d_{iso} and permitivity ϵ_{iso} are taken into account. It is assumed that electric field straight lines exist betwen secondary and primary winding as shown in the Fig. 3.21.It is also assumed that both windings are like conductive plates with linear voltage distribution.

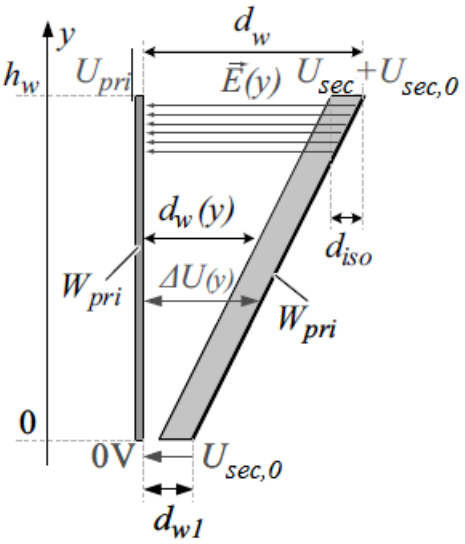

FIGURE 3.21: Calculation of Electrical energy E_{elect,R_1} between primary winding W_{pri} and secondary winding W_{sec} for funnel winding Pulse Transformer

To withstand high voltage the transformer is placed in a tank filled with oil having permitivity ϵ_{oil}.To generalize it is also assumed that the secondary winding is not earthed and thus for the differential voltage $\Delta U(y)$ the offset voltage $U_{sec,0}$ must be taken into account. Furthermore,a minimum distance of d_{w1} between winding is assumed at the bottom of the Windings.

$$\Delta U(y) = \frac{(U_{sec} - U_{prim} - U_{sec,0})}{h_w} y + U_{sec,0}. \tag{3.49}$$

$$d_w(y) = d_{oil} + d_{iso} = \frac{d_w - d_{w1}}{h_w} y + d_w 1. \tag{3.50}$$

$C = \frac{\epsilon A}{d}$, $E_{elect} = \frac{1}{2} C U^2$.

since it is assumed that electric field straight lines exist between both winding which are orthogonal to the windings, in such case the energy dE'_{elect,R_1} stored in

a differential element dy is given by

$$dE'_{elect,R_1}(y) = \frac{1}{2}\epsilon\frac{U(y)^2}{d(y)}dy. \tag{3.51}$$

$$dE'_{elect,R_1}(y) = \frac{1}{2}\epsilon\frac{((U_{sec} - U_{prim} - U_{sec,0})y + U_{sec,0}h_w)^2}{((d_w - d_{w1})y + d_{w1}h_w)h_w}. \tag{3.52}$$

By integration of the differential energy density dE'_{elect,R_1} from Equation (2.52) the energy density E'_{elect,R_1} is obtained for the area R_1, which by multiplying the perimeter length l_{R_1} leads to the electric Energy E_{elect,R_1} between the windings W_{pri} and W_{sec}.

$$E_{elect,R_1} = l_{R_1}\int_0^{h_w}\frac{1}{2}\epsilon\frac{((U_{sec} - U_{prim} - U_{sec,0})y + U_{sec,0}h_w)^2}{((d_w - d_{w1})y + d_{w1}h_w)h_w}dy. \tag{3.53}$$

Generally the electrical energy depends on the mechanical dimensions of the Pulse Transformer, the voltage difference between primary and secondary windings and the offset voltage of secondary winding [12, 31]. In case of parallel winding For different permitivity of oil and winding carrier ($\epsilon_{oil} \neq \epsilon_{iso}$), the equivalent permitivity ϵ_{equ} can be modeled as in Fig. 3.22. and can be expressed as

$$C_{equ} = \frac{C_1C_2}{C_1 + C_2} = \frac{\epsilon_1\epsilon_2 A}{\epsilon_1 d_2 + \epsilon_2 d_1} = \frac{\epsilon_{equ}A}{d}. \tag{3.54}$$

In Funnel winding transformer, since the distance between windings is not con-

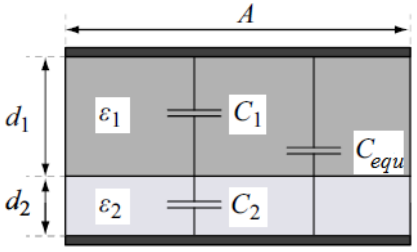

FIGURE 3.22: Finding equivalent permitivity for multiple medium between parallel plates

stant and Electric field lines path length in oil varies with y so ϵ_{equ} is function of $'y'$

$$\epsilon_{equ}(y) = \frac{\epsilon_{iso}\epsilon_{oil}(d_{iso} + d_{oil}(y))}{\epsilon_{iso}d_{oil}(y) + \epsilon_{oil}d_{iso}}. \tag{3.55}$$

Here the winding carrier thickness is assumed constant throughout the length y. Now substituting the equivalent permitivity in Equation 2.55

$$E_{elect,R_1} = \frac{l_{R_1}}{2} \int_0^{h_w} \frac{\epsilon_{iso}\epsilon_{oil}(d_{iso} + d_{oil}(y))}{\epsilon_{iso}d_{oil}(y) + \epsilon_{oil}d_{iso}} \frac{((U_{sec} - U_{prim} - U_{sec,0})y + U_{sec,0}h_w)^2}{((d_w - d_{w1})y + d_{w1}h_w)h_w} dy. \tag{3.56}$$

If the secondary winding is also grounded then offset voltage $U_{sec,o} = o$

The area R_2 is inside the winding window above secondary winding, bounded by primary winding, E-field ring and the core. To simplify the calculation of electric energy certain assumptions are made for this geometry, as shown in Fig. 3.23.

1. Primary winding is considered grounded as for high turn ratio $U_{sec} = N.U_{prim} >> U_{prim}$.

2. For uniform E-field the primary winding is extend to the core and rectangular boundary is approximated by a circular one.

3. E-field ring is assumed a circle like.

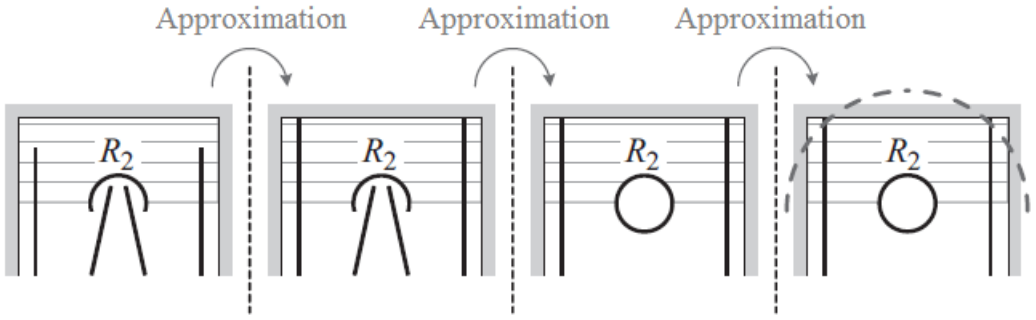

FIGURE 3.23: Simplification of the geometry over the secondary winding W_{sec} on a coaxial structure for analytical calculation of electrical energy E_{elect,R_2}

.

The whole geometry now resemble with the half coaxial structure,as shown in the Fig. 3.24. Electrical energy in region R_2 can be approximated to the half of the energy in the coaxial structure and given by

$$E'_{elect,R_2} = \frac{\pi\epsilon_{oil}(U_{sec} + U_{sec,0})^2}{4\ln(\frac{r_o}{r_r})} = \frac{\pi\epsilon_{oil}(U_{sec} + U_{sec,0})^2}{4\ln(\frac{kd}{r_r})}. \tag{3.57}$$

where $'k'$ is determined by FEM simulation, derived empirically such that the energy calculation difference between the approximated geometry and the actual

one, is minimum.

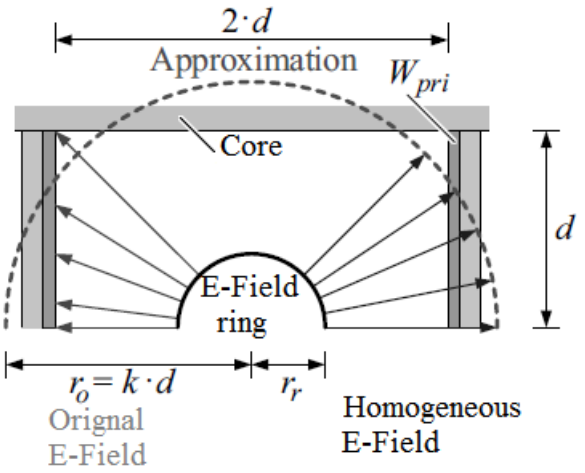

FIGURE 3.24: Approximation to a coaxial structure for the analytic Calculation of electrical energy E_{elek,R_2} using a Cylindrical capacitor

To calculate the energy for one leg of pulse transformer half of the energy of area R_2 or one quarter of the coaxial cable area energy is used. The energy E'_{elek,R_2} determined by Equation 2.57 is multiplied by the perimeter length l_{R_2} as shown in Fig. 3.20 for E_{elek,R_2}.

This area R_3 resembles with R_2 but more complex as it is not bounded by the core at one end, so to simplify the geometry, it is assumed that the primary winding is extended to the top wall of pulse transformer and also at zero potential. The resulting geometry and its approximation to coaxial structure are shown in Fig. 3.25. Further it is also assumed that the E-Field ring of secondary winding is at the center between primary winding and tank wall.

$$E_{elect,R_3} = l_{R_3} \frac{\pi \epsilon_{oil} (U_{sec} + U_{sec,0})^2}{2 \ln(\frac{kd}{r_r})}. \tag{3.58}$$

Again the factor $'k'$ is determined empirically by FEM simulation. If the tank wall is not grounded then the tank wall will be disappeared and the resulting geometry will look like a two wire shown in like Fig. 3.26 The electric energy for

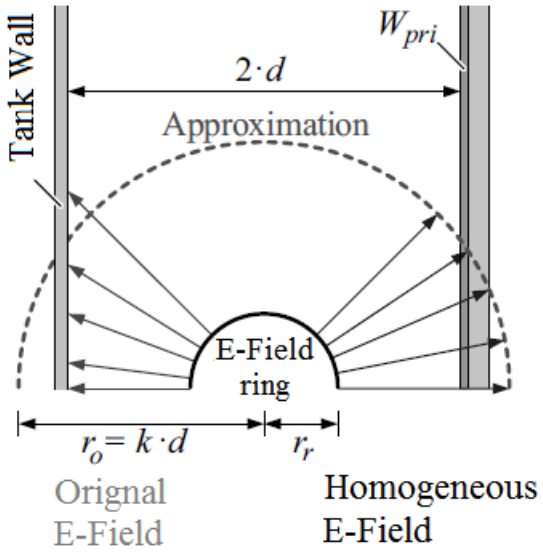

FIGURE 3.25: Approximation to a coaxial structure for the analytic Calculation of electrical energy E_{elek,R_3} using a Cylindrical capacitor

this approximation is given by

$$E_{elect,R_3} = l_{R_3} \frac{\pi \epsilon_{oil} (U_{sec} + U_{sec,0})^2}{4 \ln \left(\frac{d}{r_r} + \sqrt{(\frac{d}{r_r})^2 - 1} \right)}. \tag{3.59}$$

Area R_4 look like a nonparallel plate capacitor since distance between secondary winding and the tank wall is varying from top to bottom. The field lines in two regions, around the E-Field shaping ring and at the bottom of the secondary winding is complex and does not resemble with the nonparallel plate capacitor Field, so analytical calculation with this technique is not accurate. For more accurate calculation of electrical energy in this region, FEM simulation may be used.

The voltage on secondary winding varies linearly along the winding from top to bottom as in R_1 and distance between winding and tank wall $d_w(y)$ are expressed as

$$\Delta U(y) = \frac{U_{sec}}{h_w} y + U_{sec,0}. \tag{3.60}$$

$$d_w(y) = \frac{d'_w - d'_{w_1}}{h_w} y + d'_{w_1}. \tag{3.61}$$

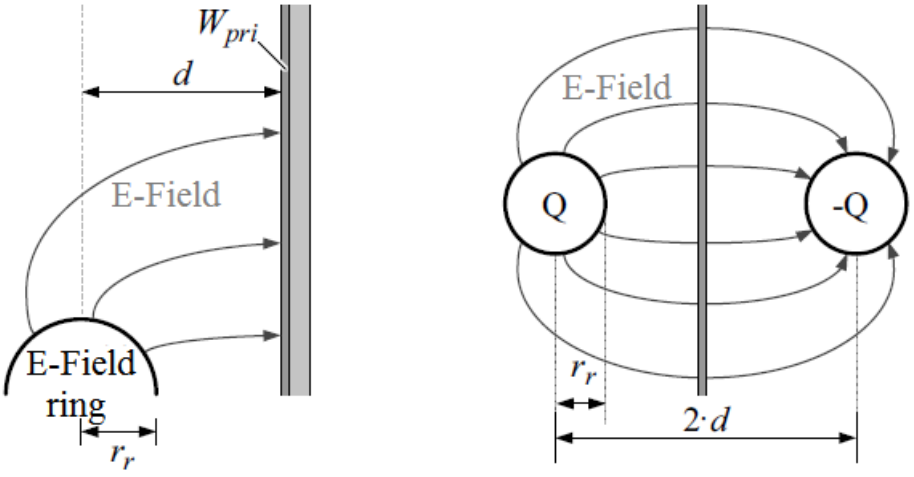

FIGURE 3.26: Approximation to a two wire line for the analytic Calculation of electrical energy E_{elek,R_3} in case of absence of Tank walls

$d'_{w_1} = 2d_w - d_{w_1}$; the electrical energy E_{elect,R_4} is calculated by

$$E_{elect,R_4} = l_{R_4} \int_0^{h_w} \frac{\epsilon_{oil}}{2} \frac{(U_{sec}y + U_{sec,0}h_w)^2}{((d_w - d'_{w_1})y + d'_{w_1}h_w)h_w} dy. \tag{3.62}$$

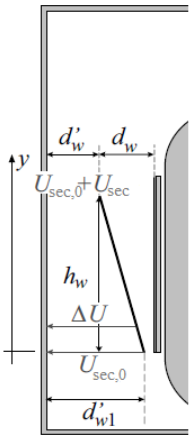

FIGURE 3.27: Variables and dimensions for area R_4 for calculation of electrical energy E_{elek,R_4}

In Fig. 3.27, the dimensions and variables for energy calculation E_{elect,R_4} of area R_4 are shown. In Funnel winding Pulse transformer the energy in R_4 has very small contribution to the total electrical energy so less accurate results may be

considered.

The area R_5 has relatively simple geometry and field lines travel vertically from secondary winding to the core as shown in Fig. 3.28. The energy calculation is similar to the R_1

$$\Delta U(x) = \frac{U_{sec}}{d_w - d_{w_1}} x + U_{sec,0}. \tag{3.63}$$

$$d(x) = \frac{h_w}{d_w - d_{w_1}} x + d_{cs,v}. \tag{3.64}$$

$$E'_{elect,R_5} = l_{R_5} \int_0^{d_w - d_{w_1}} \frac{\epsilon_{oil}(U_{sec}x + (d_w - d_{w_1})U_{sec,0})^2}{2(d_w - d_{w_1})(d_{cs,v}(d_w - d_{w_1}) + h_{wx})} dx. \tag{3.65}$$

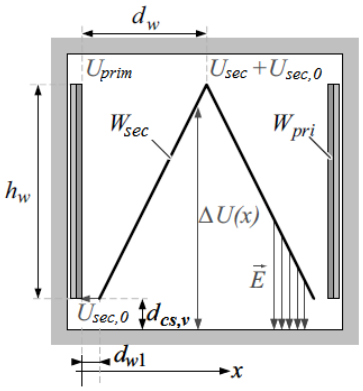

FIGURE 3.28: Variables and dimensions for area R_5 for calculation of electrical energy E_{elek,R_5}

The area R_6 has the geometry of parallel plate capacitor with two different media in between as shown in the Fig. 3.29.

$\Delta U(y) = U(y) = \frac{U_{prim}}{h_w} y$

$d(y) = d_{cp,h} = d_{oil,p} + d_{iso}$; (horizontal gap between primary winding and core)

Equivalent permitivity ϵ_{equ} of two materials is given by

$$\epsilon_{equ} = \frac{\epsilon_{iso}\epsilon_{oil} d_{cp,h}}{\epsilon_{iso} d_{oil,p} + \epsilon_{oil} d_{iso}}. \tag{3.66}$$

$dE'_{elect,R_6}(y) = \frac{1}{2}\epsilon_{equ}\frac{U(y)^2}{d(y)} dy$

Integrating this along the height y and multiplying the result by the perimeter

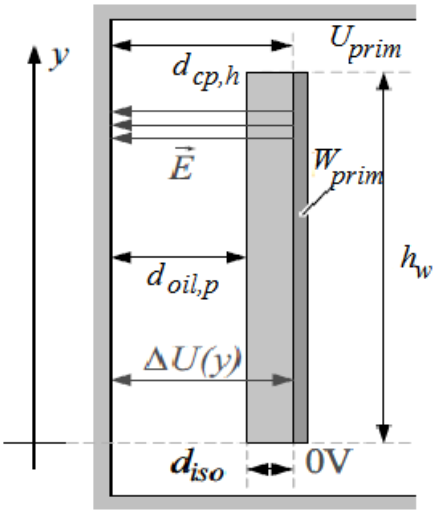

FIGURE 3.29: Variables and dimensions for area R_6 for calculation of electrical energy E_{elek,R_6}

length l_{R_6}, we get the energy for region R_6

$$E_{elect,R_6} = \frac{l_{R_6}}{6} \frac{\epsilon_{iso}\epsilon_{oil} d_{cp,h}}{\epsilon_{iso} d_{oil,p} + \epsilon_{oil} d_{iso}} U_{prim}^2. \tag{3.67}$$

3.8.2 Calculation of Leakage Inductance

Determining Leakage inductance is more difficult as compare to distributed capacitance. For leakage inductance calculation, the transformer cross section cannot be divided into different regions as in case of finding parasitic capacitance.The magnetic energy is found more precisely by FEM simulation and from this energy leakage inductance is calculated. By ampere's law

$$\oint \vec{H} dl = N_{prim} I_{prim} \implies H = \frac{N_{prim} I_{prim}}{h_k}. \tag{3.68}$$

The magnetic energy E_{mag} is given by

$$E_{mag} = \frac{1}{2}\mu \int_V H^2 dV. \tag{3.69}$$

If a uniform magnetic field is assumed between the windings then the leakage inductance L_σ is given by Equation 2.22

$$L_\sigma = \frac{1}{2}\mu \frac{N_{prim}^2 l_w d_w}{h_k}$$

Leakage inductance L_σ depends on physical parameters and the permability value of the core material. Therefor dimensioning of Pulse transformer and selection of appropriate core can minimize the $L_\sigma C_d$ product, hence minimize pulse rise time.

Chapter 4

Simulation Results

For simulation of pulse transformer to evaluate parasitic capacitance and leakage inductance FEMM (Finite element method magnetics) version 4.2 is used. Which is an open source software. FEMM is a software used to solve electromagnetic problem in two dimensional axisymmetric and planar domains. In this work two types of problems are simulated in FEMM. First is electrostatic problem, for calculation of parasitic capacitance and second is magneto static problem, for the evaluation of leakage inductance of pulse transformer.

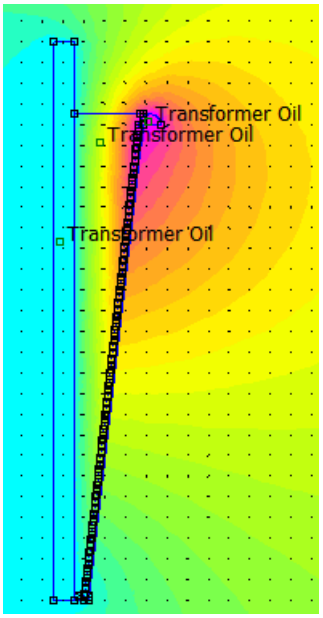

FIGURE 4.1: FEMM electrostatic simulation for region R_1 electric energy

4.0.1 FEM Simulation for Distributed Capacitance

To find parasitic capacitance electrostatic simulation of pulse transformer cross section is done and electric energy is evaluated for different regions and this per unit energy is multiplied with the corresponding depths for those regions. Total electric energy is sum of all individual region energies.The parasitic capacitance of pulse transformer is found by equating this total energy with the expression of stored energy in a capacitor. In defining the problem in FEMM, secondary wind-

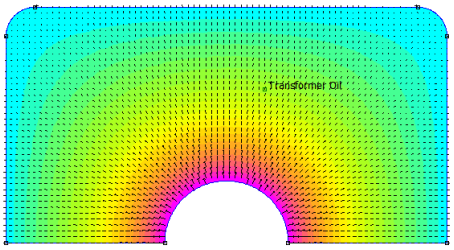

FIGURE 4.2: FEMM electrostatic simulation for region R_2 electric energy

ing of pulse transformer is assumed of 'n' conductors having different potential difference with the ground, representing turns of the secondary winding. Core and box of the transformer are assumed grounded and single turn sheet conductor is modeled for the primary winding. Transformer oil and the windings bearer are assumed to have same permitivity $\epsilon_r = 2.5$ for the simulation.

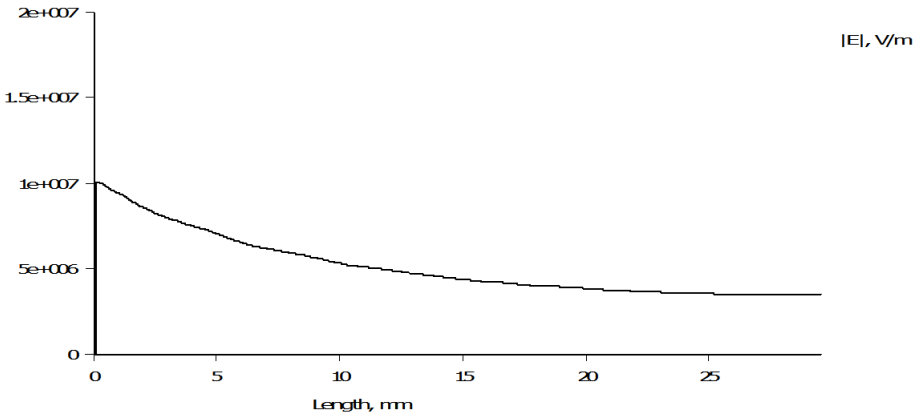

FIGURE 4.3: Electric field magnitude on a line from top of E-field ring to core wall.

Region R_1 is between secondary and primary winding. Due to funnel shape secondary winding and voltage ramp up from bottom to top turn(E-field shaping ring) electric field is not uniform. Most of the electric energy of pulse transformer is in this region thats why for rough estimate of parasitic capacitance this region is evaluated. Electric energy depends on the permitivity value of the medium between the windings in actual two materials are there one is transformer oil and other is winding bearer, which is usually craft paper. For this simulation it is assumed that both have same permitivity.

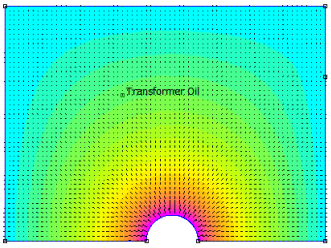

FIGURE 4.4: FEMM electrostatic simulation for region R_3 electric energy

The region R_2 is above region R_1 and bounded by primary windings of both legs,core and E-field shaping ring.For simulation Core wall is assumed grounded, primary windings at $2KV$ and secondary E-field shaping ring at $150KV$. Electric field magnitude plot shows high electric field intensity around the ring. For $150KV$ secondary voltage air breakdown is very much likely so pulse transformer is immersed in an oil tank.

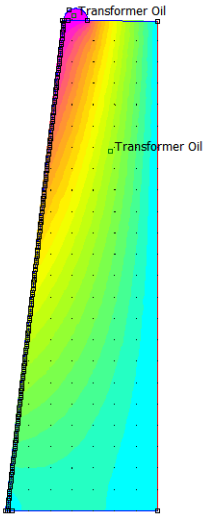

FIGURE 4.5: FEMM electrostatic simulation for region R_4 Electric energy

TABLE 4.1: FEMM Electrostatic Energy calculation for different regions of Pulse transformer

Region	**Energy (mJ/mm)**	**Depth of Region**	**Total Energy (mJ)**
R_1	0.879	515mm	452.68
R_2	0.559	236	131.92
R_3	0.383	900	344.7
R_4	0.451	920	414.92
R_5	0.037	236	8.732
R_6	$7.66 * 10^{-4}$	270	0.206

Distributed capacitance per leg of the simulated pulse transformer based on energies listed in Table2.2 is given by

$E_{elect} = \frac{1}{2} C_d V^2$

$\Rightarrow C_d = \frac{2E_{elect}}{V^2} = \frac{2(1353.158)}{(150 * 10^3)^2} = 120pF$

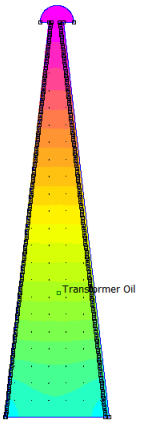

FIGURE 4.6: FEMM electrostatic simulation for Electric energy in region R_5

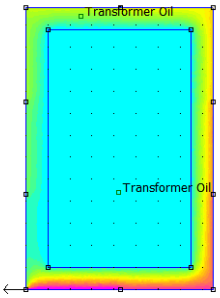

FIGURE 4.7: FEMM electrostatic simulation for region R_6 Electric energy, top view

4.0.2 FEM Simulation for Leakage Inductance

Determining leakage inductance is different and little bit difficult than distributed capacitance. In this case we cannot divide transformer cross section into different regions.magnetic energy in the space between primary and secondary winding is calculated, which correspond to the leakage flux not coupling between windings.The leakage inductance L_σ to the primary side is dependent on the found magnetic energy, primary winding current and the permeability value of the medium.

$$E_{mag} = \frac{1}{2} L_\sigma I_{prim}^2 \implies L_\sigma = 2E_{mag}/I_{prim}^2 \tag{4.1}$$

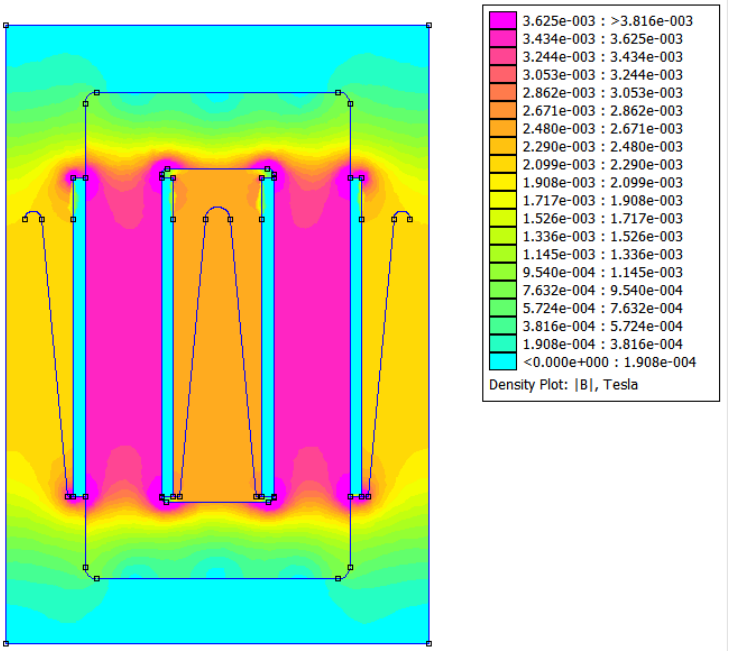

FIGURE 4.8: FEMM magnetostatic simulation,Magnetic flux density

Chapter 5

Pulse Transformer Core

Magnetic Core is used in Pulse transformers for two basic purposes. First it links the magnetic flux between primary and secondary windings, particularly if they are not overlapped. Second it increases the primary winding inductance thus decreasing magnetizing current resulting in low voltage droop and back swing. In our case, primary and secondary windings are overlapped on same transformer leg to reduce leakage inductance. Primary winding inductance may be increased by increasing number of turns but this solution will increase leakage inductance, therefore fast rise time and low voltage droop requirements are incompatible with this solution.The better solution is using a magnetic core. Selection of core material depends on various magnetic properties including saturation B_{sat} and remanent B_{rem} flux densities, resulting core losses and relative permeability μ_r. Inductance of a winding with core having relative permeability μ_r, effective length $'l'_e$, effective area $'A'_e$ and $'n'$ number of turns is given by

$$L = \frac{\mu_o \mu_r n^2}{l_e / A_e}. \tag{5.1}$$

Effective length of the core $'l'_e$ is usually taken at the midpoint of core cross section, shown as dotted line in Fig. 3.1, Chapter 2 and effective area A_e is taken if the core cross section area is varying or skin depth for fast rising pulses is taken into account.Both parameters $'l'_e$ and $'A'_e$ are given in data sheet by magnetic

core manufacturer or some time core factor $C_l = l_e/A_e$ is provided. It is evident

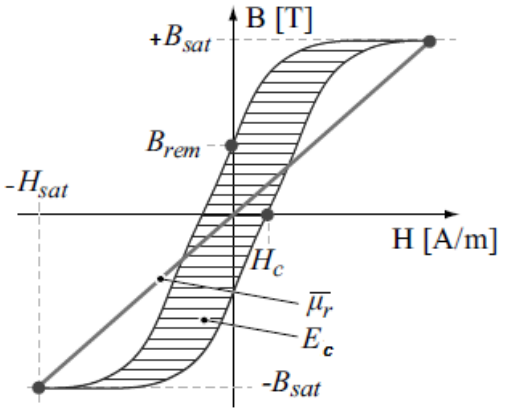

FIGURE 5.1: Magnetic materials characteristic properties

by Equation 4.1 that Inductance of a winding can be increased by increasing number of turns or by using a core with higher relative permeability value μ_r.For this purpose special magnetic materials with high relative permeability has been developed.

Using higher permeability core, seems to be a simple solution but there is a problem associated with this. Skin depth, thickness the magnetic flux will penetrate inside the core with permeability μ and conductance σ for an oscillating magnetic field with frequency $'\omega'$ is given by

$$\delta = \sqrt{\frac{2}{\omega\mu\sigma}}. \tag{5.2}$$

It is evident from Fig. 5.2 that for fast rising pulses, the magnetic flux will penetrate less in high permeability core materials, due to skin depth, causing less effective area A_e and effective permeability. This effect can be reduced to some extent if the resistivity of core material is kept high, can be achieved by using ferrite core or by laminating core.

Another problem is that permeability is not constant due to nonlinear relation between B and H in magnetic materials as shown in Fig. 5.1. Pulse permeability depends on the particular region of the $B-H$ loop, the transformer is operating during the pulse [9]. For uni-polar pulses small excursion made by the core on B-H loop.These small loops will move upward for series of unipolar pulses, untill the increase and decrease in B is same. At this stage the residual B at the end

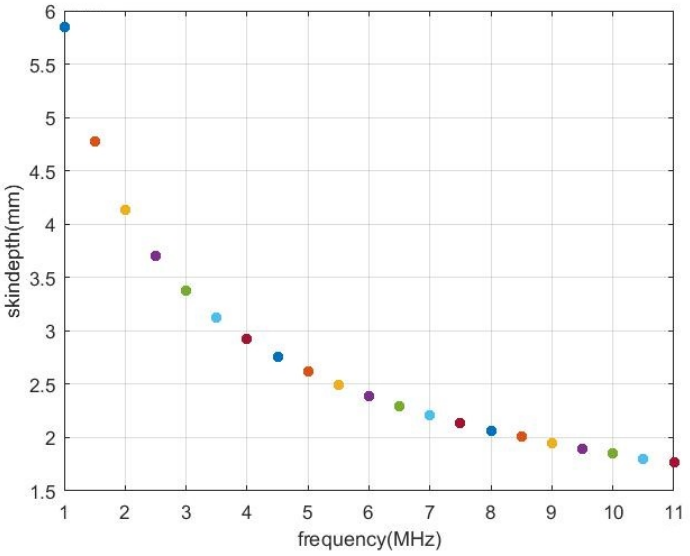

FIGURE 5.2: Core Skin depth variation for higher frequency components

of the pulse is called remanent flux density B_{rem}. If B_{rem} is very high then there are chances that maximum flux density B_{max} exceeds B_{sat} and transformer core get saturated. In that case the pulse permeability and hence winding inductance would fall to a very low value.

For constant amplitude V_p pulse with duration t_p, applied to n turn winding with cross section area A, change in flux density during pulse is given by [13]

$$\Delta B = \int_0^{t_p} \frac{V_p}{nA} dt = \frac{V_p t_p}{nA}. \tag{5.3}$$

The condition to avoid core saturation is

$$B_{sat} > B_{rem} + \Delta B = B_{max}. \tag{5.4}$$

There are many ways to avoid core saturation in addition to using a core material with higher value of B_{sat}. It is clear from Equation 5.3 that for a fixed volt-second product $V_p t_p$, change in magnetic flux density ΔB can be reduced by increasing number of turns n or by using a core with larger cross section area A. Core saturation can also be avoided by keeping B_{rem} to a lower value for this an opposite polarity pulse is applied to the winding or on a separate winding on the same core after the pulse duration t_p. Core reset is explained in detail in next section.

5.1 Pulse Transformer Core Reset

In Pulse transformer, operating with uni polar pulses, magnetic flux swings only in one direction, not fully utilizing the core. To avoid saturation at minimum twice size core cross section is required in uni polar pulse operation as compare to bipolar operation without core reset [32]. To achieve flux swing from -ve to +ve during the pulse, core reset circuits are used, which are mainly classified into two categories

1. DC Reset Circuit
2. Active Reset Circuit (active components with energy recovery)

In this work, DC reset is studied. In DC reset circuit, a dc current is flown in primary or secondary or reset winding in a direction such that it produces flux in the core in opposite direction to the flux produced by the primary winding pulse as shown in the Fig. 5.3. The DC reset circuit premagnetizes the core to a negative flux density before the start of pulse to achieve bipolar operation of the core. A DC reset circuit consists of DC power supply U_{reset},an inductor/choke $L_{choke}$to protect DC supply from HV pulses and reset winding with turns N_{reset} as shown in Fig. 5.4. Choke resistance R_{choke} and R_{com} are shown for power losses calculations.

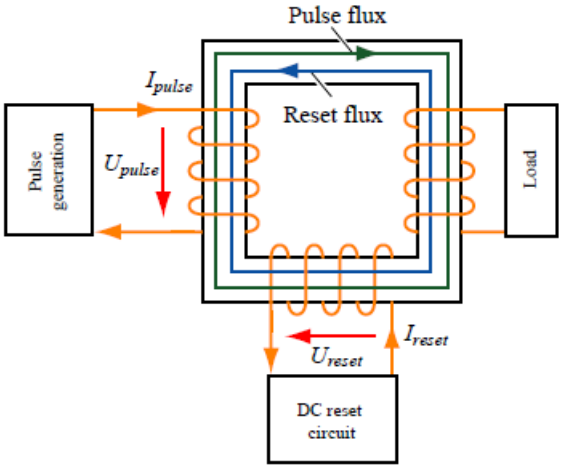

FIGURE 5.3: Block diagram showing DC reset flux in pulse transformer core with pulse generator and load

Pulse power system with reset circuit would have additional losses due to reset

power supply,reset winding and choke as compare to system without reset circuit. It has certain advantages in terms of smaller pulse transformer core resulting in lesser pulse transformer copper losses and improved rise time specs by offering lesser distributed capacitance and leakage inductance. Pulse power system without reset have less components like choke,extra power supply and third winding etc and they consume no power to waste in these components. On the other hand without reset system minimum twice the core cross section would be required and it will have $\sqrt{2}$ times "longer winding,copper losses,leakage inductance,distributed capacitance and pulse rise time"

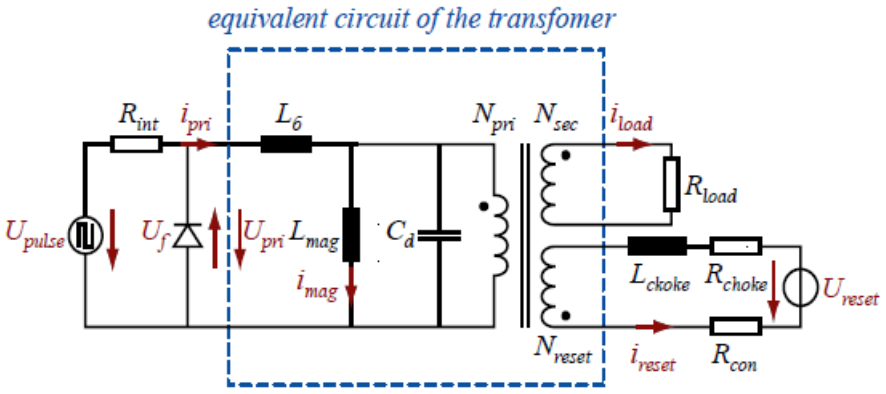

FIGURE 5.4: A general pulse power system showing reset winding in pulse transformer

To understand DC rest operation Pulse timing diagram is divided into three portions S_1, S_2 and S_3 as shown in Fig. 5.5. The period T1 in time section S1 is equal to the pulse width. T2 is the time after the pulse in which the freewheeling diode is conducting and T3 is the period between the end of freewheeling and the next pulse.

In Fig. 5.6, B-H curve of a pulse transformer with and without pre-magnetization is shown. For symmetric core operation DC reset offers double change of magnetic flux density ΔB without saturation so reduces the core area to half as compare to without reset pulse transformer offering same ΔB.

Designing of Choke coil plays crucial role in the performance of DC reset circuit. To make reset circuit energy efficient losses must be minimized and optimal choke inductor should be designed.For simulation AMCC1000 core is selected, which can be used for $20MW$ Klystron modulator pulse transformer reset [33].

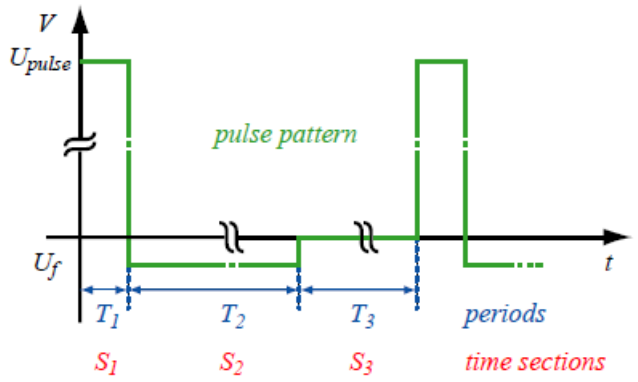

FIGURE 5.5: A common pulse timing diagram with different sections

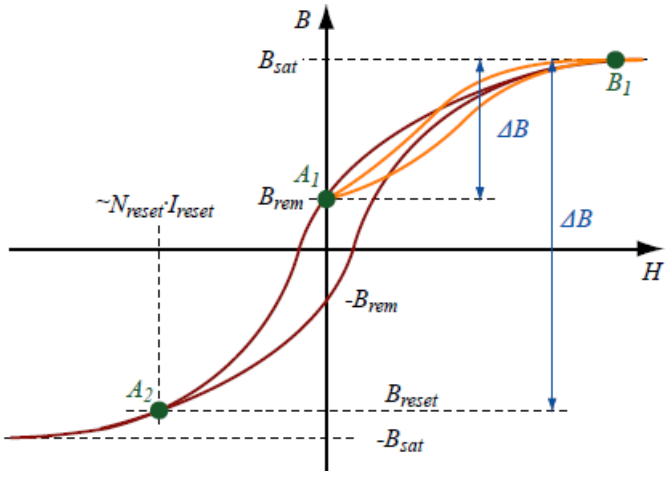

FIGURE 5.6: B-H curve of a Pulse Transformer with and without reset pre-magnetization

Fig. 5.7 shows magnetic flux densities vector plot for the said core at $50A$ of DC current through 132 turns. Air-gape length is varied from $0.5mmto4mm$ and its effect on coil inductance is observed. For a Choke coil around a core with air-gape length δ the inductance L_{choke} is given by

$$L_{choke} = \frac{N_{choke}^2}{R_m} \approx \frac{N_{choke}^2 \mu_o A_{core}}{\delta}. \tag{5.5}$$

Due to fringing effect the field is not uniform and the inductance calculated by Equation 4.5 is not accurate so FEM simulation is used to find the inductance value. In Fig. 5.8, the coil inductance obtained by FEMM simulation and calculated values are ploted vs air-gap length. For small air-gape the simulated

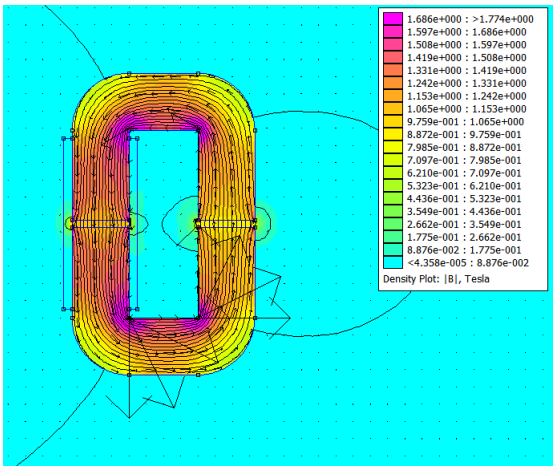

FIGURE 5.7: FEMM Simulation of Magnetic Flux density vector plot for Reset Choke with 4mm air-gap

calculated results deviate a lot. So Equation 4.5 approximation can be used for inductance calculation for large air-gapes only.

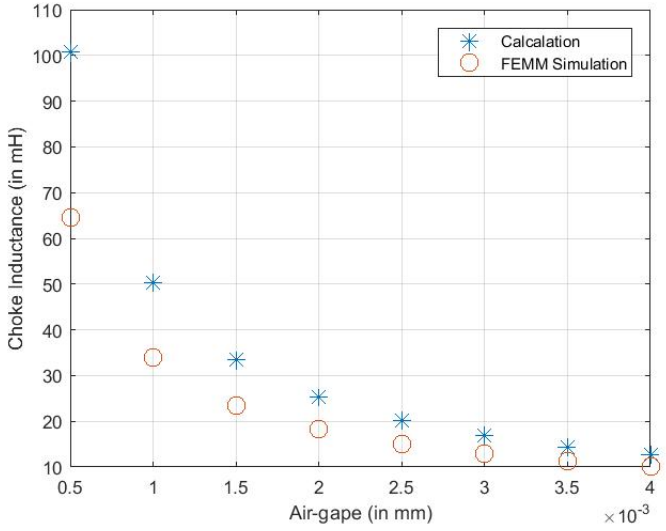

FIGURE 5.8: Choke inductance vs Air-gap length variation calculation and FEMM simulation comprision

In choke inductor designing it must be considered that the time constant for the DC current to reach the peak value will be larger for higher inductance values, so reset time will be more. In medical LINAC, the duty cycle is usually very low, as the microwaves pulse width is few microseconds and OFF time is in milliseconds, therefore heavy inductor choke for reset may not cause any problem. In other applications where pulse repetition rate is very high like Radars, large inductor choke may not be used in reset circuits.

Chapter 6

Conclusion and Future Work

6.1 Conclusion

In evaluating distributed capacitance we observed that major portion of electrostatic energy, responsible for distributed capacitance is in two regions. One is between primary and secondary winding and the second region is between secondary winding and pulse transformer tank walls. If size limitations are relaxed then transformer tank walls can be further away from secondary winding using bigger tank. This would serve two purposes, one is reducing distributed capacitance and second is providing more space for cooling, making thermal design more easy. Leakage inductance evaluated by magnetostatic energy are much reduced by funnel shape winding as compared to parallel winding topology. Simulation Results of Leakage inductance and distributed capacitance are slightly higher than Bortis et al results [34]. As mentioned by Bortis et al that actual values of distributed capacitance and leakage inductance were slightly higher than his simulation results, when measured after construction of pulse transformer [34]. So our results are closer to actual measured values. The design procedure for evaluation of parasitic elements of pulse transformer can be utilized for variety of loads including Klystron, Magnetrons and plasma applications. Due to Dependence of effective

permeability on frequency of input power, same evaluation procedure can be repeated for different values of permeability.

6.2 Future Work

Motivation behind this research work, was the project of particle accelerator for medical applications. In medical LINAC, Klystron and Magnetrons are used as high power microwave source. Stability in magnitude, frequency and phase of RF power is required for more accurate dose delivery to cancer patients. To derive these vacuum tubes high voltage high current pulse power supplies called modulators are required. In modulator Pulse transformer play a vital role to full fill the pulse voltage requirements for stable operation of particle accelerators. This research work contribute towards dimensioning of pulse transformer before it is constructed so that pulse parameters requirements are met. Pulse parameters like rise time, overshoot, flat top stability, voltage droop and tail undershoot are discussed and their dependence on pulse transformer parasitic elements are described. Three types of Pulse transformers are compared for fast rise time and the best one i-e funnel winding is selected for detail analytical model and FEM simulations. Electrostatic and Magntostatic FEMM simulations for electric energy and magnetic energy respectively are used to find distributed capacitance C_d and leakage inductance L_σ. Software used for FEM simulations is FEMM(Finite element method megnetics). It is a two dimensional(2D) FEM software. Since Pulse transformer is symmetric in structure, so 2D FEM simulation results for different regions electric energies are multiplied with their corresponding depths results in better approximation of the totall electric energy. For magnetic energy of pulse transformer, magnetostatic problem is selected in FEMM. The magnetic energy in a plane between primary and secondary windings is used to calculate Leakage inductance, for this purpose whole pulse transformer cross section is simulated. Dimensions of the pulse transformer simulated are chosen for 150 KV klystron modulator at CERN. Results obtained are in conformity with the Bortis et al work [34] with the factor of relative permeabilty value used for transformer oil as

Bortis et al used air permitivity value for simulations. In future three dimensional FEM software like COMSOL and ANSYS-MAXWELL 3D will be used for more accurate evaluation of pulse transformer parasitic elements evaluation.

Pulse Transformer core reset is studied and DC reset is explained with FEMM simulation of Choke required for DC reset. In future Active reset techniques will be explored for energy recovery to make the modulator more energy efficient. As the motivation behind this research is development of particle accelerators for medical applications, therefore future research may include control loops for stabilization of beam and RF frequency for more accurate dose delivery.

Bibliography

[1] C. Karzmark, C. S. Nunan, and E. Tanabe, *Medical Electron Accelerators*. McGraw-Hill, 1993, vol. 1, pp. 89-104.

[2] E. Schamiloglu, R. J. Barker, M. Gundersen, and A. A. Neuber, "Modern pulsed power: Charlie martin and beyond," *Proceedings of the IEEE*, vol. 92, no. 7, pp. 1014–1020, 2004.

[3] D. Bortis, J. Biela, and J. W. Kolar, "Optimal design of a two-winding inductor bouncer circuit," *IEEE Transactions on Plasma Science*, vol. 38, no. 10, pp. 2716–2724, 2010.

[4] N. Carleto and C. Motta, "Design, construction and characterization of a line-type pulse modulator for driving high power magnetron," in *Microwave and Optoelectronics, 2005 SBMO/IEEE MTT-S International Conference on*. IEEE, 2005, pp. 330–333.

[5] R. Rosol, P. Adraktas, R. Barlow, E. Carlier, L. Ducimetière, P. Faure, A. Fowler, J. Schipper, L. Sermeus, and M. Stjepic, "Design and development of a 6.25 kv/1 ka pfn to supply the new ps booster distributor magnets," in *Pulsed Power Conference (PPC), 2013 19th IEEE*. IEEE, 2013, pp. 1–5.

[6] G. N. Glasoe and J. V. Lebacqz, *Pulse Generators*. McGraw-Hill, 1948, vol. 3, pp. 499-555.

[7] F. Arntz, M. Gaudreau, K. Ostlund, M. Kempkes, and J. Casey, "New concepts for pulsed power modulators: Implementing a high voltage solid-state marx modulator," in *Power Modulator and High Voltage Conference (IPMHVC), 2012 IEEE International*. IEEE, 2012, pp. 28–30.

[8] R. Cassel, "Pulsed voltage droop compensation for solid state marx modulator," in *IEEE International Power Modulators and High Voltage Conference, Proceedings of the 2008.* IEEE, 2008, pp. 117–119.

[9] G. E. Fish, "Soft magnetic materials," *Proceedings of the IEEE*, vol. 78, no. 6, pp. 947–972, 1990.

[10] M. Akemoto, S. Gold, A. Krasnykh, and R. Koontz, "Pulse transformer R&D for NLC klystron pulse modulator," in *Pulsed Power Conference, 1997. Digest of Technical Papers. 1997 11th IEEE International*, vol. 1. IEEE, 1997, pp. 724–729.

[11] D. Aguglia, C. Martins, M. C. Bastos, D. Nisbet, D. Siemaszko, E. Sklavounou, and P. Viarouge, "Klystron modulator technology challenges for the compact linear collider (clic)," in *Pulsed Power Conference (PPC), 2011 IEEE.* IEEE, 2011, pp. 1413–1421.

[12] F. Pan, L. Jin, P. Pan, and Z. Xu, "Design procedure of the leakage inductance for a pulse transformer considering winding structures," *IEEE Transactions on Plasma Science*, vol. 45, no. 9, pp. 2504–2510, 2017.

[13] P. W. Smith, *Transient Electronics: Pulsed Circuit Technology.* Oxford, UK: John Wiley & Sons, 2011, vol. 1, pp. 137-168.

[14] S. Jang, Y. Son, J. Oh *et al.*, "Perveance monitor for measuring an 80-mw klystron characteristics," *Interface*, vol. 500, p. 10V, 2004.

[15] H.-J. Eckoldt, "Long pulse modulators," *arXiv preprint arXiv:1607.01572*, vol. 03, 2016, pp. 45-53.

[16] S. Gold, "Klystron gun arcing and modulator protection," in *Presented at*, no. SLAC-PUB-10435, 2001, p. 19.

[17] R. Zeng, A. Johansson, K. Rathsman, and S. Molloy, "Influence of the droop and ripple of modulator on klystron output," *ESS Technical notes ESS/AD/0033, European Spallation Source AB*, vol. 43, 2011, pp. 344-356.

[18] C. Rong, Y. Jianhua, X. Cheng, and P. Zilong, "Research of a fractional-turn ratio saturable pulse transformer and its application in a microsecond-range pulse modulator," *Plasma Science and Technology*, vol. 19, no. 6, p. 064014, 2017.

[19] M. Jaritz, S. Blume, and J. Biela, "Design procedure of a 14.4 kv, 100 khz transformer with a high isolation voltage (115 kv)," *IEEE Transactions on Dielectrics and Electrical Insulation*, vol. 24, no. 4, pp. 2094–2104, 2017.

[20] D. Bortis, G. Ortiz, J. W. Kolar, and J. Biela, "Design procedure for compact pulse transformers with rectangular pulse shape and fast rise times," *IEEE transactions on Dielectrics and Electrical Insulation*, vol. 18, no. 4, pp. 1171–1180, 2011.

[21] *IEEE standards for Pulse Transformers*, IEEE Std., 1987, vol. 1, pp. 33-56.

[22] J. Oh, M. Cho, W. Namkung, K. Chung, T. Shintake, and H. Matsumoto, "Rise time analysis of pulsed klystron-modulator for efficiency improvement of linear colliders," *Nuclear Instruments and Methods in Physics Research Section A: Accelerators, Spectrometers, Detectors and Associated Equipment*, vol. 443, no. 2-3, pp. 223–230, 2000.

[23] T. Duerbaum and G. Sauerlaender, "Energy based capacitance model for magnetic devices," in *Applied Power Electronics Conference and Exposition, 2001. APEC 2001. Sixteenth Annual IEEE*, vol. 1. IEEE, 2001, pp. 109–115.

[24] A. Massarini, M. Kazimierczuk, and G. Grandi, "Lumped parameter models for single-and multiple-layer inductors," in *Power Electronics Specialists Conference, 1996. PESC'96 Record., 27th Annual IEEE*, vol. 1. IEEE, 1996, pp. 295–301.

[25] J. Biela and J. W. Kolar, "Using transformer parasitics for resonant converters-a review of the calculation of the stray capacitance of transformers," in *Industry Applications Conference, 2005. Fourtieth IAS Annual Meeting. Conference Record of the 2005*, vol. 3. IEEE, 2005, pp. 1868–1875.

[26] J. Biela, D. Bortis, and J. W. Kolar, "Analytical modeling of pulse transformers for power modulators," in *Power Modulator Symposium, 2006. Conference Record of the 2006 Twenty-Seventh International*. IEEE, 2006, pp. 135–140.

[27] W. F. J. Crewson, M. R. Lindholm, and D. K. Woodburn, "Power modulator," May 18 1999, uS Patent 5,905,646.

[28] W. Crewson, "A new solid state high power pulsed modulator," vol. 34, 2001, pp. 573-581.

[29] W. Crewson and D. Woodburn, "Power modulator having at least one pulse generating module; multiple cores; and primary windings parallel-connected such that each pulse generating module drives all cores," May 25 2004, uS Patent 6,741,484.

[30] M. Akemoto, Y. Chin, Y. Sakamoto *et al.*, "High-power klystron modulator using solid-state igbt modules," in *Proceedings of the Second Asian Particle Accelerator Conference, Beijng, China*, 2001, pp. 618–620.

[31] P. Viarouge, D. Aguglia, C. Martins, and J. Cros, "Modeling and dimensioning of high voltage pulse transformers for klystron modulators," in *Electrical Machines (ICEM), 2012 XXth International Conference on*. IEEE, 2012, pp. 2332–2338.

[32] R. Adler, J. Stein, B. Ashcraft, and R. Richter-Sand, "Improvements in pulse transformer performance achieved using pulsed reset circuitry," in *Pulsed Power Conference, 1997. Digest of Technical Papers. 1997 11th IEEE International*, vol. 1. IEEE, 1997, pp. 616–620.

[33] D. Bortis, J. Biela, and J. W. Kolar, "Optimal design of a dc reset circuit for pulse transformers," in *Applied Power Electronics Conference, APEC 2007-Twenty Second Annual IEEE*. IEEE, 2007, pp. 1171–1177.

[34] D. Bortis, "20MW halbleiter-leistungsmodulator-system," Ph.D. dissertation, ETH Zurich, 2009, pp. 230-307.